Marine and Petroleum Geology 147 (2023) 105981

Contents lists available at ScienceDirect

Marine and Petroleum Geology

journal homepage: www.elsevier.com/locate/marpetgeo

Sources and migration pathways of methane and light hydrocarbons in the subsurface of the Southern Po River Basin (Northern Italy)

Andrea Ricci [a,*], Stefano Cremonini [b], Paolo Severi [c], Franco Tassi [d,e], Orlando Vaselli [d,e], Andrea Luca Rizzo [a,f], Antonio Caracausi [a], Fausto Grassa [a], Jens Fiebig [g], Bruno Capaccioni [b,1]

[a] Istituto Nazionale di Geofisica e Vulcanologia (INGV), Sezione di Palermo, Via Ugo La Malfa 153, 90146, Palermo, Italy
[b] Department of Biological, Geological and Environmental Sciences, University of Bologna, Piazza di Porta S. Donato 1, 40127, Bologna, Italy
[c] Geological, Soil and Seismic Area of the Emilia-Romagna Region, Viale Della Fiera 8, 40127, Bologna, Italy
[d] Department of Earth Sciences, University of Florence, Via G. La Pira 4, 50121, Florence, Italy
[e] CNR-IGG Institute of Geosciences and Georesources, Via G. La Pira 4, 50121, Florence, Italy
[f] Istituto Nazionale di Geofisica e Vulcanologia (INGV), Sezione di Milano, Via Alfonso Corti, 12, 20133, Milano, Italy
[g] Institut für Geowissenschaften, Goethe-Universität, Altenhöferallee 1, 60438, Frankfurt Am Main, Germany

ARTICLE INFO

Keywords:
Methane
Po river basin
Emilia-romagna region
Natural gas geochemistry
Hydrocarbon source rocks
Gas accumulation and migration
Thermogenic gas
Microbial gas

ABSTRACT

This paper presents new chemical and isotopic data on gases from deep oil and gas fields, bubbling gases, dissolved gases in groundwaters and dry seeps of the Southern Po River Basin (Emilia-Romagna, Italy), aiming to (i) characterize and differentiate the various types of deep natural gases; (ii) identify the source(s) of methane and light hydrocarbons in shallow aquifers and surface gas-rich emissions; (iii) propose a conceptual model of natural fluid migration pathways in the sedimentary prism of the Southern Po River Basin. Based on the isotopic composition of CH_4 and C_2–C_4 n-alkanes, $CH_4/(C_2H_6+C_3H_8)$ ratio, relative proportion of the C_7 hydrocarbons and relative concentration of cyclic compounds with respect to the total cyclic abundance, three main deep reservoirs of hydrocarbons are identified in the subsurface of the Southern Po River Basin: (1) microbial gas hosted in Pliocene-Pleistocene marine sediments, (2) thermogenic gas hosted in Miocene deposits and (3) thermogenic gas produced in Triassic carbonates. Helium isotopes of these deep fluids indicate an almost pure crustal origin (Rc/Ra values = 0.014–0.04), with negligible contributions from mantle-derived helium. A variable contribution of atmosphere-derived fluids is highlighted by low $^{4}He/^{20}Ne$ (down to 5.42) and $^{40}Ar/^{36}Ar$ ($\leq$319.5) values. Comparison of chemical and isotopic signatures of deep and surficial hydrocarbon occurrences suggests that methane in shallow groundwaters or gas seeps is sourced by microbial gas migrating upward from deep Plio-Pleistocene reservoirs, with no detectable contributions of Triassic or Miocene thermogenic hydrocarbons. At shallow depths (roughly around 20–50 m.b.g.l.), Plio-Pleistocene microbial methane appears to be mainly stored in anoxic aquifers. However, where CH_4 further migrates upwards and reaches aerobic environments (e.g., aquifers or soils), it readily undergoes a process of exothermic microbial oxidation mediated by methanotrophic bacteria. Where the structural architecture of the sedimentary sequence favors the migration of fluids, the methanotrophic biofilter is bypassed and CH_4 is discharged through soil diffuse degassing or gas bubbling at water wells. We argue that microbial consumption might be able to bio-sequester significant amounts of Plio-Pleistocene deep-sourced methane in the form of CO_2 and biomass. Such process might be widespread in the subsurface of the Southern Po River Basin and, possibly, in other foreland basins worldwide.

1. Introduction

With a globally averaged surface dry air mole fraction of ≈1900 ppb in September 2021 (https://gml.noaa.gov/ccgg/trends_ch4/), methane (CH_4) is the most abundant hydrocarbon in the atmosphere, where it plays a fundamental role in the tropospheric chemistry. Natural methane sources include wetlands, animals, wildfires, terrestrial permafrost, oceans and other water bodies (lakes, ponds and rivers) and

* Corresponding author.
E-mail address: andrea.ricci@ingv.it (A. Ricci).

[1] Dedicated to the memory of our colleague and friend, Bruno Capaccioni who passed away in September 2016.

https://doi.org/10.1016/j.marpetgeo.2022.105981
Received 12 July 2022; Received in revised form 14 October 2022; Accepted 16 October 2022
Available online 27 October 2022

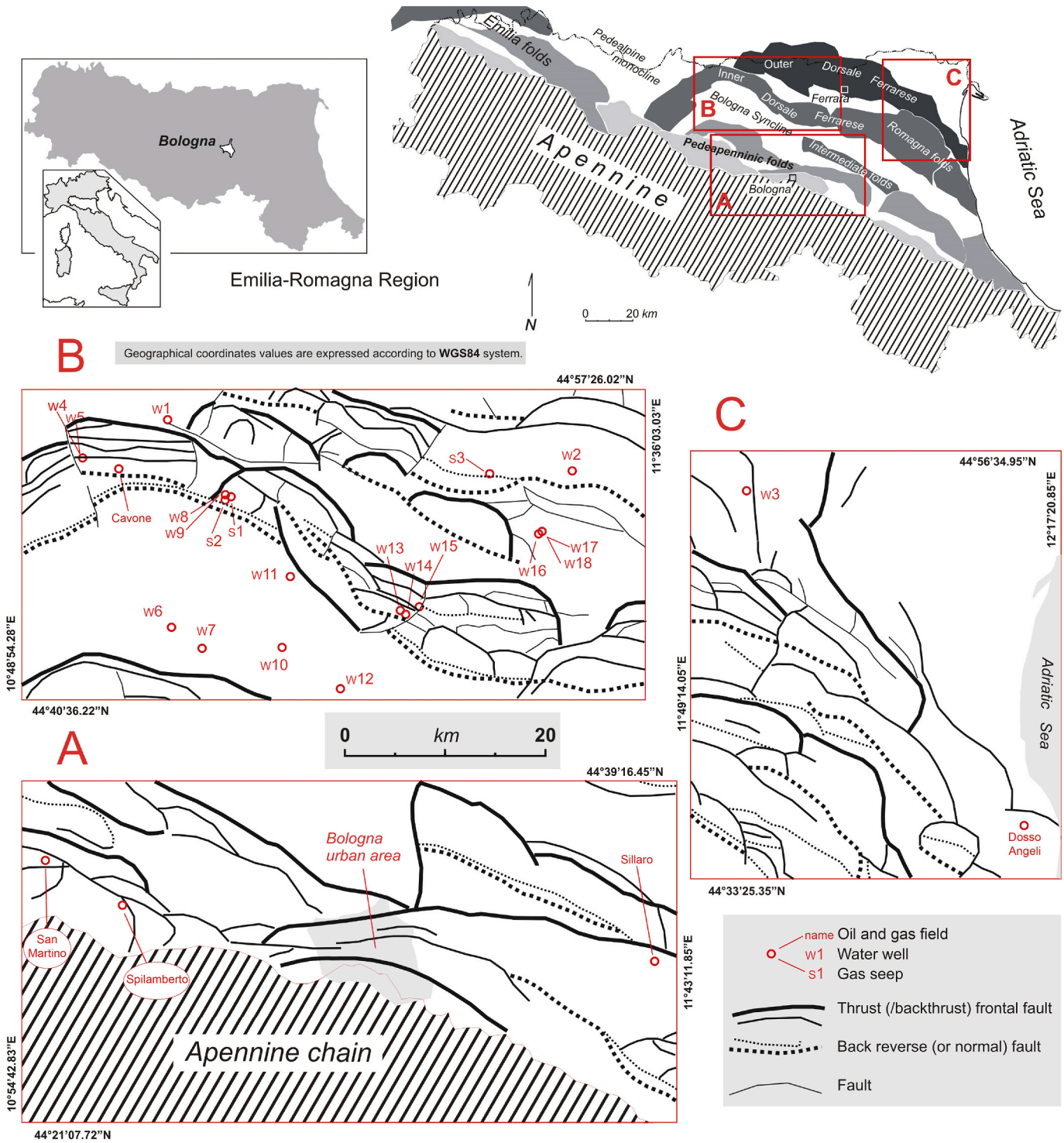

Fig. 1. Main groups of buried tectonic structures of Emilia-Romagna Region. A, B, C) Detail of buried tectonic structures (after Cerrina Ferroni et al., 2002; simplified) and study-points location. White areas are the major depocentral synclines and the padealpine monocline. The gray-tones areas highlight the various buried thrusts envelope and only poses a descriptive geometrical value.

geological sources such as terrestrial and marine gas seeps, mud volcanoes, geothermal areas and active volcanoes (Saunois et al., 2020). Geological sources have long been considered to play a minor role in the global CH_4 cycle but recent studies, providing more accurate estimates, highlighted their importance in the overall methane budget (Etiope, 2009). Sedimentary basins account for 90% (Etiope and Klusman, 2002) of the total geogenic CH_4 emission. In rapidly subsiding basins, deposition and accumulation of sediments eroded from high-relief areas form km-thick sedimentary sequences. Organic matter buried with sediments is biodegraded by metabolic activity of microbial consortia (biogenesis) and thermochemically transformed by heat and pressure through cracking and reforming reactions (thermogenesis). Methane is produced by mechanisms where biogenic gases exhibit significantly higher $CH_4/(C_2H_6 + C_3H_8)$ ratios and lighter $\delta^{13}C$–CH_4 than those of thermogenic gases (Whiticar, 1999). Microbial activity and maturation of organic matter are responsible for the production of methane (and minor

amounts of higher hydrocarbons) in the subsurface. In tectonically active basins, fracture and fault systems strongly enhance channeling and vertical migration of CH_4-rich fluids from the source zone to reservoirs (Mucciarelli et al., 2015), ultimately allowing their seeping from terrestrial and submarine vents (Etiope, 2009; Capaccioni et al., 2015). Surface seepage of methane, light hydrocarbons and oil is a widespread phenomenon along the Alpine-Himalayan Orogen where mud volcanoes, dry gas vents and brackish/salt water seeps, mostly occurring in correspondence of suture zones between converging plates (e.g. Gulf of Cadiz, Mediterranean Ridge, Makran, Northern Apennines, Carpathians, Caucasus, Black Sea and Caspian Sea) discharge large volumes of CH_4 and C_{2+} volatile organic compounds (VOCs) into the atmosphere (Kopf et al., 2001, 2003; Delisle et al., 2002; Somoza et al., 2003; Baciu et al., 2007; Bonini et al., 2013). These surficial seeps are intimately linked to both subsurface hydrocarbon accumulations and tectonic regime. Inland and offshore natural seeps of biogenic and thermogenic gases have been documented in Italy where they punctuate the Apennine orogenic front, from the Po Plain to Sicily (Etiope et al., 2007; Capozzi and Picotti, 2002; Bonini, 2007; Bonini et al., 2013). The Southern Po River Basin (Emilia-Romagna Region, Italy), a syntectonic sedimentary wedge forming the infill of the Pliocene-Pleistocene foredeep of the Northern Apennine, still preserves major CH_4 reservoirs at the core of the main buried thrust groups (Casero, 2004; Martinelli et al., 2012a), which are presently exploited by oil and gas companies (e.g., ENI Ltd., Gas Plus Ltd.). At the Southern Po River Basin, fluid seepage feeds surficial diffuse and punctual emissions of CH_4-rich gases and produce CH_4-saturated shallow aquifers (Martinelli et al., 2012a and reference therein; Capaccioni et al., 2015). The outermost buried front of the Northern Apennine orogenic thrust belt (Ferrara arc) is still tectonically active, in response to the general compressive stress field dating from the Middle Pleistocene, the most recent seismic sequences occurred in May 2012 and February 2022. In relation to the two main seismic shocks of 20 and 29 May 2012, co-seismic and post-seismic phenomena, such as sudden water temperature increases (up to 55 °C) and strong gas bubbling in shallow phreatic wells, as well as extrusions of sediment-water-gas mix from surficial fractures and old sealed gas wells, occurred within the epicentral region (Bonzi et al., 2017). These events have been reported to occur for several years after the seismic sequence. However, their relation with the local seismicity and the origin of the fluids associated to the majority of these unusual phenomena are still unclear.

The relation between seismicity and fluid circulation has been demonstrated in different sectors of the Apennines (e.g., Chiodini et al., 2011, 2020; Di Luccio et al., 2018; Buttitta et al., 2020; Chiarabba et al., 2022). The Southern Po River Basin, as proven by the 2012 seismic sequence and the fluids-associated co- and post-seismic phenomena, is a seismically active area where a clear relation between fluid circulation and seismicity has been observed (Bonzi et al., 2017; Pezzo et al., 2018). In this framework, it is fundamental for the ongoing and future studies on role of fluids in earthquake triggering to geochemically constrain deep sources and shallow occurrences of fluids and to have a robust reference model of fluid migration pattern.

In this study, we investigate the chemical and isotopic composition of gases and waters from oil and natural gas wells, shallow groundwaters and surficial gas emissions of the Southern Po River Basin (hereafter, SPRB), with the aim of characterizing and differentiating the various types of deep natural gas accumulations and providing insights into the source(s) of methane and light hydrocarbons shallow occurrences. Finally, on this basis, a preliminary comprehensive conceptual model of natural gas reservoirs and fluid migration pathways in the SPRB subsurface is proposed.

2. Southern Po river basin (SPRB)

2.1. Geological setting

The Po River sedimentary basin (Fig. 1) is a complex physiographic and sedimentary system representing the foreland basin of both the Alps and Apennine Mountain chains (Fantoni and Franciosi, 2009). The Apennine chain is the domain of the Alpine orogen generated during the last (*Neo-Alpine*) phase of the orogenesis (Vai, 2001), linked to the collisional overthrusting of the Sardinia and Corsica continental block onto the African Apulia (Castellarin et al., 1992). After the Burdigalian and Messinian tectonic phases (Castellarin, 2001; Ghielmi et al., 2010), a fast NE-warding migration of the northern Apennine chain front toward the present location, occurred in the Lower Pliocene (Cerrina Ferroni et al., 2002). The continuation of the orogen tectonic evolution, during the Late Pliocene and Pleistocene (post-collisional phase) was due to a slab-retreat mechanism (e.g., Scrocca et al., 2007; Picotti and Pazzaglia, 2008; Martelli et al., 2017a, b) that induced a frontal area shortening and a back-arc area extension (Doglioni et al., 1999). These tectonic actions shaped a still evolving thrust-and-fold chain whose last, youngest foredeep basin is the Po valley sedimentary prism. The chain shows two fronts, 50 km apart from each other. The inner front raises above the regional alluvial plain whereas the outermost one is still buried beneath the Po Plain. The former defines the geomorphologic features of the foothill (Boccaletti and Martelli, 2004; Boccaletti et al., 2011) and coincides with the Pedeapenninic Thrust Front (PTF) (Boccaletti et al., 1985) resting, in turn, upon a first group of buried folds and thrusts very close to the PTF (Pedeapenninic folds). The latter buried front consists of three groups of main faulted folds, each coupled with a huge back syncline; from NE to SE: i) Emilia Folds, ii) Ferrara (and Romagna) Folds, iii) Adriatic Folds (Pieri and Groppi, 1981; Bigi et al., 1990; Turrini et al., 2014). The second fold group, named *Dorsale Ferrarese*, is in the central part of Emilia Romagna Region and its front is the most protracted in the foreland area. The compressive field stress, causing the thrusting, maintained the entire Apennine orogen below the coeval sea bottom up to the end of the Lower Pliocene. During the Middle-Late Pliocene (ca. 3.9–3.3 My: *Intrazanclean*) and the Lower Pleistocene (ca.2.4–2.2 My: *Gelasian*) tectonic phases (Di Dio, 1998), the chain begun to uplift and generated an embryonal emerged topography. Concomitantly with these tectonic phases, the three buried structural arches of the Emilia-Ferrara-Adriatic Folds were activated (Ghielmi et al., 2013), highlighting a tectonic *jump* of the chain front (Martelli et al., 2017b). At the end of the Lower Pleistocene, the generalized uplifting of the chain begun to trigger a quick forced marine regression all over the Po Valley moving from western toward eastern areas (Muttoni et al., 2003; Gunderson et al., 2014). Following, an important stratigraphic body (Po Valley *Prograding Complex*) was generated, with its upper coastal sands (0.8–0.65 My BP) marking the definitive physiographic change of the Po Valley area from marine to prevailing continental environment (Di Dio, 1998). At the same time, the emerged chain front also established itself at the present location (Bartolini, 2003). Finally, from the Middle Pleistocene up to the Holocene, the mainly continental sedimentation, conventionally comprised in the *Emiliano-Romagnolo Supersyntheme* (e.g., Di Dio, 1998; RER, 2003; Boccaletti et al., 2011), recorded both alluvial environment and transitional-shallow marine facies (Martelli et al., 2017b) laterally and vertically organized according to the transgressive-regressive glacio-eustatic cyclicity (Amorosi et al., 2008, 2016; Campo et al., 2017). Their fine-grained sequences were attributed to both interglacial and glacial ages. A transversal tectonic faulting of the buried thrusts (Nardon et al., 1991; ISPRA, 2015) and an order of magnitude decrease of the compressional deformation during the Pleistocene are known (Boccaletti et al., 2011) coupled with a prevailing vertical motion of buried structural highs during the Middle-Upper Pleistocene (Ghielmi et al., 2013) at about 250−230 ky BP (Martelli et al., 2017b). In the last 1.4 My, the uplifting rate of the external buried front decreased from 0.53 to 0.16 mm/y (Scrocca et al., 2007), whereas the emerged morphologic front of the chain is currently uplifting at a rate of 1 mm/y (D'Anastasio et al., 2006; Carminati and Valditacca, 2010a). The geologic subsidence rate of the Po alluvial basin in the same period is in the range of 0.5–2 mm/y (Carminati and Martinelli, 2002). Due to these movements the

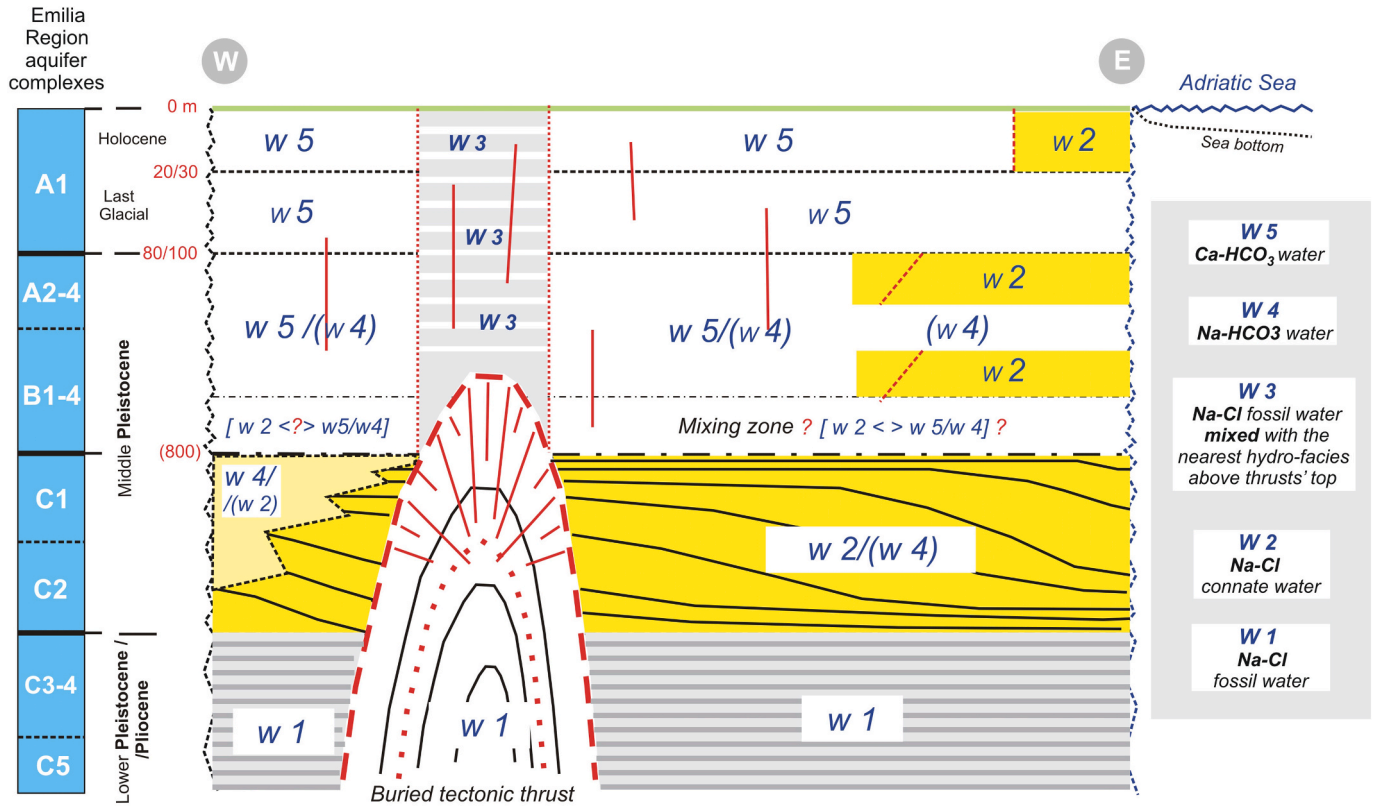

Fig. 2. Essential linedraw (not to scale) of hydrochemical facies and their hypothetic mutual relationships at depth in Emilia-Romagna alluvial plain (redrawn and modified after Moggia, 2016). The depth scale shows average values. Aquifer Complexes of Emilia Region are after RER and ENI-AGIP (1998). The thick yellow bank is the Prograding Complex Auctorum. The straight red segments suggest fractures or faults. (For interpretation of the references to colour in this figure legend, the reader is referred to the Web version of this article.)

thrusts' top of the *Dorsale Ferrarese* is now buried ~100 m deep beneath the present topographic surface (RER and ENI-AGIP, 1998; Capaccioni et al., 2015). GPS data show that the crustal shortening still occurs along the buried chain front (Devoti et al., 2010; Carminati et al., 2010) as well as the thrusting activity (Di Bucci and Angeloni, 2013; Vannoli et al., 2014). The latter was stressed by the May 2012 Emilia seismic sequence (Galli et al., 2012; Cesca et al., 2013; Ventura and Di Giovambattista, 2013; Martelli et al., 2017b; Nespoli et al., 2018) and responsible for positive vertical displacements ranging between 73 and 150 mm (Devoti, 2012; Borgatti et al., 2012) and related crustal shortening between 30 and 40 mm (Galli et al., 2012) recorded in the epicentral area.

2.2. Hydrogeological and hydrochemical setting

The Po River sedimentary basin is a system where buried marine sediments with fossil saltwater and overlying freshwaters-bearing continental sediments are still mutually interplaying (Castellarin et al., 2006; Martinelli et al., 2016). The hydrostratigraphic framework of the Emilia foreland basin was derived by the interpretation of industrial seismic sections and hydrocarbon and water well logs analysis, allowing the recognition of a repeated alternance of fine-grained aquiclude/aquitard bodies and relatively coarse-grained aquifers (RER and ENI-AGIP, 1998; Teatini et al., 2006). At the SPRB, the aquifers are the sum of continental river channel bodies with related subfacies (hydrostratigraphic unit A and B in RER and ENI-AGIP, 1998) and Pleistocene costal sands (hydrostratigraphic unit C in RER and ENI-AGIP, 1998). In the paleo-marine domain, lying beneath the SPRB aquifers, they are mainly represented by the coarse-grained term of turbidite sequences. In principle, the formers have a more irregular geometry and contain freshwater, whereas the latter are more regular and contain brackish or salt waters. As a matter of fact, the hydrostratigraphic boundaries between freshwater and saltwater cut diagraphically the boundaries of the three main aquifers (Groups A, B, and C) schematically drawn in Fig. 2. In fact, the deepest aquifer (C), corresponding to the last marine deposits and to the transitional complex, is now often bearing freshwater rather than the original marine connate saltwater, thus suggesting water displacement phenomena. The elevation of the buried freshwater/saltwater boundary changes from one place to another, mainly according to the local tectonic features, being deeper in synclines and higher in anticline-top areas (IRSA and CNR, 1982; RER and ENI-AGIP, 1998; Molinari et al., 2007). The elevation of this boundary is higher along the present back-coastal Adriatic areas, due to the presence of recent connate marine waters. At some locations, the occurrence of brackish water uprisings is recorded, especially in areas lying in the inner alluvial plain, far from the sea, coinciding with buried structural highs as well as synclines (Castellarin et al., 2006), leaving open questions concerning the water uprising mechanisms and pathways. According to RER and ENI-AGIP (1998), the aquifer Group A is characterized by Ca–HCO_3 waters with the exception of two areas: i) the easternmost part of the Region together with the *Dorsale Ferrarese* top where Na–HCO_3 groundwaters are recorded and ii) the highest culminations of the *Dorsale Ferrarese* thrust hosting Na–Cl waters. The underlying aquifer Group B is not completely known, and this explains the uncertainties in the sketch of Fig. 2. The central-eastern part of the Region holds Na–HCO_3 waters whereas in the western part, the presence of predominantly Ca–HCO_3 groundwaters is poorly known. In Group C, the Na–HCO_3 and/or Ca–HCO_3 groundwaters are likely due to a displacement of a possible original Na–Cl hydrochemical facies. The Na excess in Na–HCO_3 waters is due to ionic exchanges between meteoric waters and Na-rich clay minerals together with the mediation of CO_2, mainly deriving from the organic matter degradation (RER and ENI-AGIP, 1998) and/or the Na–Ca exchange with clays (Martinelli et al., 2014).

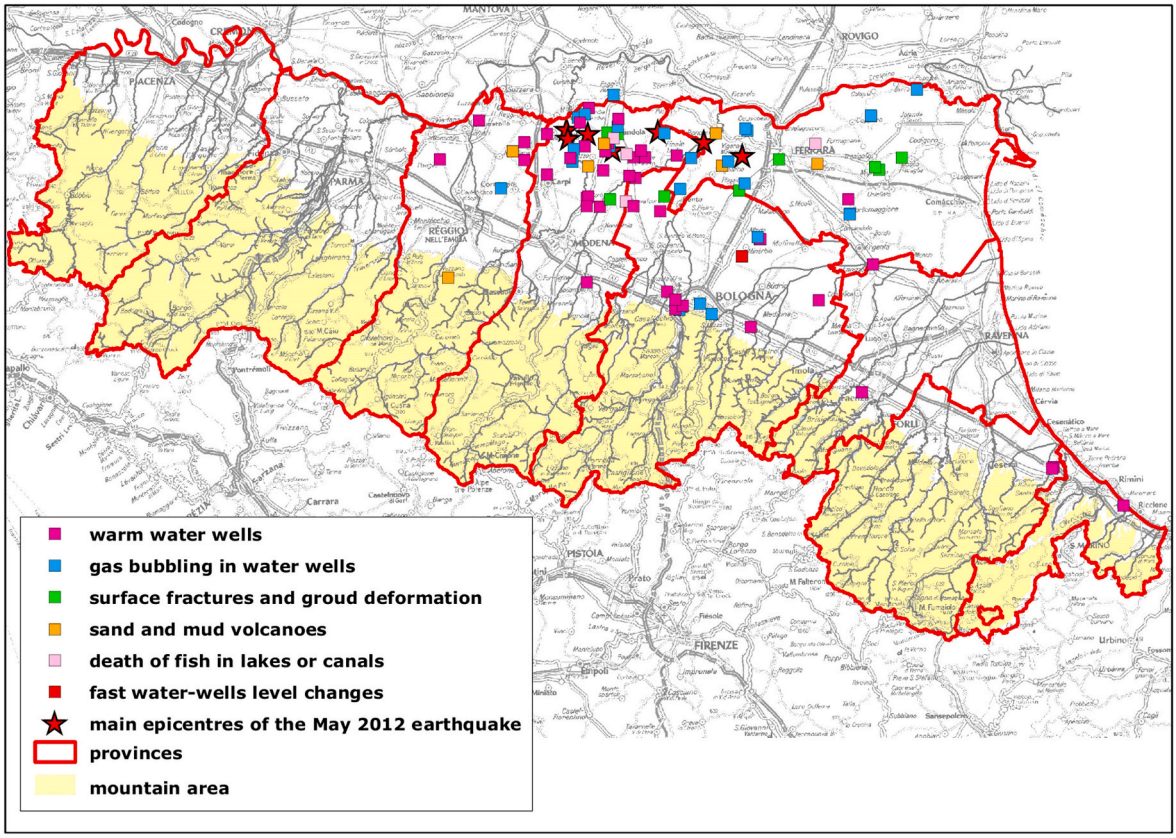

Fig. 3. Unusual Geological Phenomena (UGP) location in Emilia-Romagna Region occurred between May 2012 and September 2018.

Table 1
Location of study sites. The geographical coordinates of oil and gas fields refer to a generic gas field baricentral point. Type, depth, details and location with respect to the tectonic setting of the investigated sites are reported. Details: A.1 = gas bubbling in brackish/salt water; A.2 = gas bubbling in freshwater; B = CH_4-rich water; C = unaltered domestic phreatic well (reference point); D = dry gas seepage from soil; E = gas seepage from a human-induced sediments-fluid eruption; WWW = Warm Water Wells. Tectonic setting: PF = Pedeapenninic folds; ITG = Intermidiate thrust group; DFI = Dorsale Ferrarese inner frontal thrust group; DFO = Dorsale Ferrarese outer frontal thrust group; and IS = Interposed syncline. na = not available.

Name	ID	Type	WGS84-N; WGS84-E	Well/reservoir depth (m. b.g.l.)	Details	Tectonic setting
Cavone	–	Oil field	44°52′57.83″; 10°56′38.91″	2900	–	DFI
Spilamberto	–	Gas field	44°32′25.14″; 11°01′27.83″	1242–1460	–	PF
San Martino	–	Gas field	44°35′01.03″; 10°55′44.38″	na	–	PF
Sillaro	–	Gas field	44°29′36.88; 11°41′48.06″	2100	–	ITG
Dosso Angeli	–	Gas field	44°35′39.16″; 12°14′48.51″	2885–3839	–	DFO
Vallalta	W1	Abandoned gas well	44°55′47.91″; 11°00′01.42″	1742	A.1	DFI
Diamantina	W2	Abandoned gas well	44°53′08.39″; 11°30′33.90″	≈200	A.1	DFO
Ambrogio	W3	Abandoned gas well	44°54′32.27″; 11°53′44.60″	≈350	A.1	DFO
Novi	W4	Phreatic well	44°53′20.30″; 10°52′53.40″	8.5	WWW	DFI
Novi	W5	Artesian well	44°53′19.93″; 10°52′55.88″	25	B	DFI
Sorbara	W6	Phreatic well	44°44′40.04″; 11°00′16.53″	12	WWW	IS
Bomporto	W7	Phreatic well	44°43′32.64″; 11°02′31.02″	8	WWW	IS
Camurana	W8	Phreatic well	44°51′53.10″; 11°04′18.65″	10	WWW	DFI
Camurana	W9	Artesian well	44°51′52.29″; 11°04′19.37″	22	B	DFI
Crevalcore	W10	Phreatic well	44°43′28.96″; 11°08′42.88″	5.7	WWW	IS
Camposanto	W11	Phreatic well	44°47′14.99″; 11°09′12.06″	10	WWW	DFI
Decima	W12	Phreatic well	44°41′15.09″; 11°13′08.90″	7	C	IS
Renazzo	W13	Phreatic well	44°45′34.88″; 11°17′30.57″	6.5	A.2	DFI
Corpo Reno (Casino del gas)	W14	Phreatic well	44°45′22.38″; 11°18′09.03″	4.5	A.2	DFI
Corpo Reno	W15	Phreatic well	44°45′47.57″; 11°19′08.35″	5.5	A.2	DFI
Mirabello (C7)	W16	Phreatic well	44°49′33.91″; 11°27′56.63″	7	WWW	DFO
Mirabello (C5bis)	W17	Phreatic well	44°49′39.77″; 11°28′11.08″	4.5	WWW	DFO
Mirabello (C5)	W18	Phreatic well	44°49′39.77″; 11°28′11.08″	5	WWW	DFO
Warm Grounds of Medolla (WGM)	S1	Gas seepage	44°51′13.41″; 11°05′09.22″	–	D	DFI
Bruino (CPT)	S2	Gas seepage	44°51′28.64″; 11°04′33.34″	24	E	DFI
Bondeno (CPT)	S3	Gas seepage	44°52′50.51″; 11°24′31.96″	20	E	DFO

The Na–Cl waters derive from mixing processes between Quaternary transgressive saltmarsh and lagoonal or Pliocene marine waters and meteoric waters (Martinelli et al., 2014). Following recent surveys (e.g., Moggia, 2016), Fig. 2 shows a simplified and ideal sketch of the groundwater chemical facies distribution. Tritium and ^{14}C measurements indicate that the maximum age of the oldest waters (Groups A and B) is in the order of 30 ky BP (Martinelli et al., 2014), although the ages can result renewed by severe artificial water withdrawal (ENI-AGIP, 1998). Notwithstanding this, it is accepted that the deeply buried Pliocene Po basin sediments are still experiencing an active dewatering process highlighted by the expulsion of brackish waters (*salt plumes*) from the buried thrusts front (Martinelli et al., 2016). Furthermore, it was also recognized that in the central-eastern part of the Emilia plain the deep confined aquifers not recharged by modern infiltration circuits are characterized by a high hydraulic head possibly linked to the active tectonic compression (Martinelli et al., 2016) as suggested for the Hungarian Plain (Toth and Almasi, 2001).

2.3. Unusual geological phenomena (UGP) in the SPRB

In May–June 2012, Emilia-Romagna was struck by an intense seismic sequence, affecting a 50-km wide area located at the southern edge of the Po River alluvial plain. The sequence started on May 20, with a M_L 5.9 earthquake followed by thousands of aftershocks, six of them with $M_L \geq 5.0$. Once the seismic sequence began, several anomalous events, presently known as unusual geological phenomena (UGP) were observed and reported by the local population (BonziFerrari et al., 2014; 2017). From June 2012 to September 2018, 88 UGP have been documented, mostly occurring in the epicentral area of the seismic swarm and few of them in peripheral areas, e.g., the municipality of Bologna and the eastern sector of the Po Plain (Fig. 3). These UGP were grouped into six categories, where the number of events is reported in brackets, as follows: (i) occurrence of warm water in phreatic wells (41); (ii) gas bubbling in water wells (24); (iii) surficial fractures and ground deformations (9); (iv) fast water-wells level changes (2); (v) fish deaths in small lakes and canals (4) and (vi) activation of sand and mud volcanoes (8). Most UGP concerned the increase of water temperature, up to 55 °C, in phreatic wells less than 10 m deep and mainly located north of Modena. These events were called "Warm Water Wells" and the acronym WWW will be used from now on to refer to these phenomena. Some WWW were found to be linked to a malfunctioning of water well pumps (Bonzi et al., 2017) but the great majority of such events seemed to be related to still unknown natural mechanisms. An online database (http://ambiente.regione.emilia-romagna.it/geologia/temi/geologia/fenomeni-geologici-particolari) was created by the Geological, Seismic and Soil Survey of the Emilia-Romagna Region to collect all the information regarding the UGP and make the data available for everyone to access. It is worth noting that UGP in the Po Plain have long been known by the local population. A notable example is located in the vicinity of the town of Medolla, a small municipality located within the epicentral area of the 2012 seismic sequence, where subcircular areas with anomalously high ground temperatures and soil diffuse degassing have been reported since the late nineteenth century (Capaccioni et al., 2015 and reference therein) and have been named with the toponym *Terre Calde di Medolla* (literally Warm Grounds of Medolla, hereafter WGM).

3. Materials and methods

3.1. Sampling sites

The study sites are located at the SPRB, most of which are within the Modena province. Water and gas samples were collected from 15 domestic phreatic and artesian wells and 3 abandoned gas wells (W-sites), 3 gas seepages (S-sites) and 14 exploitation wells from 5 oil and gas fields (Table 1). At wells W4, W6, W7, W8, W10, W11, W16, W17 and W18 at least one episode of water temperature increase has been documented after the seismic sequence of May–June 2012. It is worth noting that gas seepage S1, namely "Warm Grounds of Medolla" (WGM), an area characterized by anomalously high ground temperatures and CH_4 diffuse degassing, has been known since the late nineteenth century. The basic information concerning the surveyed sites and their location with respect to the buried tectonic setting are summarized in Table 1. As for the oil and gas wells, also the W- and S-sites are mostly located in structural highs, but a small group is in syncline areas (Fig. 1). The Cavone field (Pieri and Groppi, 1981; Nardon et al., 1991; ENI, 1994) produces oil from a structural trap lying in the Dorsale Ferrarese inner arc. The reservoir is hosted in the Mesozoic carbonate formations (*Brecce di Cavone* and *Calcari Grigi di Noriglio*) at around 3000 m depth. Spilamberto and San Martino gas fields (ENI, 1994) lie upon the Pedeapenninic folds group. At Spilamberto, a first gas reservoir was intercepted at 1242 m depth, lying at the bottom of the Pliocene clayey seal, while a further productive level was located at 1460 m depth (Scicli, 1972). The main gas reservoir at Sillaro field is located at 2100 m depth in several horizons hosted in the Pliocene suite (Energy-pedia, 2010). The reservoir of Dosso Angeli (ENI, 1972) is hosted in an anticline structural trap in the Pliocene sandy deposits. It consists of 8 reservoirs with the gas-water contact lying at a depth between 2885 and 3839 m (Simeoni et al., 2017). The well W1 (Vallalta) was originally created as a gas well but today is out of service and delivers gases (mostly methane) from the Miocene geological formations together with waters mainly supplied by the uppermost 250 m of the Quaternary sedimentary cover (Martinelli et al., 2016). The well W2 (Diamantina) is one of 24 abandoned gas wells drilled up to an average depth of 200 m between 1948 and 1963 (Scicli, 1972). This well erupted gas and brackish water in 2014 after the degraded sealing disruption. At Coccanile (close to the village of Ambrogio), 24 gas wells were drilled between 1944 and 1969 up to an average depth of 350 m (Scicli, 1972). In 2013 one of these wells (W3) erupted warm and brackish water and gases as the result of sealing wear. The depth of the water wells W4–W18 was not exceeding 25 m and are located in the Holocenic sedimentary suite (<20 m) and within sediments dating back to the Middle-Upper Pleistocene (20–350 m). They intercept A and, to a lesser extent, B regional aquifers (Fig. 2).

3.2. Water and gas sampling

Water and dissolved gas samples from phreatic wells were collected using sampling equipment consisting of a Rilsan® tube (6 mm in diameter) lowered to half of the water column and connected to a 150 mL syringe equipped with a three-way valve to pump the water up to the surface. Waters and gases from artesian wells were sampled using a submerged electric pump. Water samples were collected after the displacement of a water volume triple than the inner volume of the tube (Cabassi et al., 2013 and references therein). Pre-evacuated 250 mL glass flasks equipped with a Teflon stopcock were used for the dissolved gas sampling. Glass flasks were connected to the Rilsan® tube or submerged into a filled bucket for sampling of phreatic and artesian wells, respectively. After the opening of the stopcock, water was allowed to enter up to about three quarters of the flask's inner volume (Tassi et al., 2009). Gases naturally bubbling in water wells were collected using a funnel positioned up-side-down and connected to pre-evacuated 50–60 mL glass flasks. In order to detect temporal compositional variations and trends in the period 2015–2016, water and gas sampling at W4, W5, W8, W9, W10, W11 and W12 were performed every two months. Waters from deep exploitation wells were collected with a water-gas separator, while gases were sampled by connecting the sampling line to the pressure-control valve of the production wells. At each exploitation wells, two gas aliquots were collected, as follows: (1) a pre-evacuated 60 mL glass flask for the determination of concentrations of major compounds and isotopic composition of C_1–C_4 n-alkanes, and (2) a 12 mL glass vial equipped with a silicone rubber porous septum for the analysis of C_5–C_{10} VOCs. At eight selected wells, a third gas aliquot for the

Table 2
Chemical and isotopic composition of waters from G and W sites. Concentrations of the main solutes and TDS are expressed in mg/L. Isotopic compositions of O and H, and C are reported in delta notation (‰) relative to V-SMOW and V-PDB, respectively. na = not available; bdl = below detection limit.

Name/ID	Date	T	pH	Eh	EC	TDS	HCO_3^-	F^-	Cl^-	Br^-	NO_3^-	SO_4^{2-}	Na^+	NH_4^+	K^+	Mg^{2+}	Ca^{2+}	δD-H_2O	$\delta^{18}O$–H_2O	$\delta^{13}C$-TDIC
	d.m.y.	°C		mV	μS/cm	mg/L	mg/L	mg/L	mg/L	mg/L	mg/L	mg/L	mg/L	mg/L	mg/L	mg/L	mg/L	‰	‰	‰
Cavone	04/04/2016	na	7.5	−324	49000	32692	542	3.9	18624	97	bdl	782	11943	bdl	161	153	323	3.7	7.7	−7
Spilamberto	04/04/2016	na	6.9	−88	75500	50966	58	1.4	30988	151	bdl	4.7	17171	bdl	188	899	1505	−9.8	−0.01	−5
San Martino	04/04/2016	na	6.7	−129	na	594	247	0.5	134	bdl	bdl	6	71	bdl	27	7	101	−33.9	−3.3	
Sillaro	14/10/2016	na	7	−120	88900	63328	232	8.9	37434	189	bdl	9.8	21616	bdl	246	1244	2348	−4.1	1	
Dosso Angeli	03/02/2016	na	6.9	−118	na	71015	156	2.7	43291	218	bdl	157	23343	bdl	140	1102	2605	0.3	0.06	−13.1
W1	28/06/2017	18	7.7	−180	na	4475	610	0.6	2146	10.6	14.3	34	1434	43	10	104	69			
W2	11/07/2014	21	7.3	−192	na	6874	214	0.8	3765	20	bdl	7	2269	bdl	18	323	252	−69.2	−10	
W3	21/02/2013	25	7.4	−220	na	25590	381	2	15785	69	bdl	15	7768	50	36	901	582	−57.1	−8	
W4	23/03/2016	10.1	7	15	1135	1062	598	0.1	87	0.06	5.4	117	58	bdl	5	55	137			−16.7
	16/05/2016	15	7.2	−86	1000	1093	665	0.08	73	0.04	4.1	96	56	0.05	3	48	148			
	29/06/2016	14.9	7	127	1227	1007	552	0.11	91	0.03	8.3	100	59	0.15	6	52	138			
	02/09/2016	17.1	7	45	1160	1047	622	0.17	71	0.04	1.8	99	52	0.16	4	51	145			
	02/11/2016	15.3	7.2	79	1108	1032	610	0.11	63	0.04	4.2	92	52	0.43	7	56	147			
W5	16/05/2016	14.8	7.3	−191	1246	1445	961	0.29	74	0.1	1.5	69	30	1.07	3	73	232			−24.8
	29/06/2016	16.3	7.2	−230	1358	1043	701	0.12	66	0.16	bdl	39	29	0.24	3	63	142			
	02/09/2016	15	7.3	−228	1304	1256	854	0.17	62	0.07	0.2	48	28	0.79	3	64	195			
	02/11/2016	14.6	7.1	−225	1315	1279	866	0.25	59	0.08	0.1	39	33	0.91	4	69	208			
W6	02/09/2016	30.3	7.2	31	1632	1434	729	0.2	99	0.1	7	216	98	bdl	65	68	152			
W7	20/09/2016	22.2	7.2	52	1638	1466	800	0.22	153	0.17	1.5	114	90	1.27	118	82	106			
W8	22/10/2015	53.6	7.3	104	1429	1390	631	0.19	203	0.71	1.8	125	68	1.14	140	68	150			
	28/10/2015	32.7	7.3	100	1519	1436	658	0.3	206	0.67	1.7	132	69	1.33	145	71	151			
	23/03/2016	12.5	7.4	14	2060	1974	568	0.13	564	1.82	31.7	165	314	3.35	92	60	173			−17.2
	16/05/2016	14.6	7.1	80	2145	1934	756	0.15	383	1.44	18.4	168	279	bdl	69	60	198			
	29/06/2016	14.6	7.1	127	1963	1513	653	0.13	250	0.67	9.6	147	225	bdl	57	43	127			
	02/09/2016	15	7.2	66	1402	1221	644	0.85	109	0.23	1.1	120	67	0.24	95	58	126			
	02/11/2016	15.9	7.2	155	1320	1201	653	0.15	89	0.18	1.9	104	80	bdl	100	52	120			
W9	28/10/2015	14.7	7.3	−250	3031	2865	1165	0.61	753	3.35	0.5	76	540	10.45	7	120	188			
	23/03/2016	12.7	8.1	−367	2560	2422	753	0.16	883	3.54	2	7	488	9.16	7	116	153			−26.9
	16/05/2016	14.8	7.6	−306	2410	2471	1354	0.39	411	1.89	0.05	2	384	9.78	9	111	188			
	29/06/2016	15.2	7.4	−366	4180	3082	1051	bdl	955	3.95	bdl	125	613	9.94	10	122	192			
	02/09/2016	15.2	7.5	−323	3500	2676	1092	1.39	773	3.2	2.3	14	493	9.72	11	107	170			
W10	28/10/2015	31.4	7.6	54	1058	1000	574	0.3	48	0.18	29.9	69	50	1.34	62	47	119			
	23/03/2016	19.7	7.9	−14	811	702	359	0.17	39	0.09	60.7	61	46	0.04	41	29	66			−16.1
	03/05/2016	32.8	7.8	−24	899	805	382	0.2	69	0.12	66.2	62	45	bdl	43	36	102			−14.6
	11/05/2016	33.8	7.9	−88	910	854	454	1.22	39	0.12	56.2	68	46	0.23	49	37	103			−17.3
	29/06/2016	20.4	7.4	83	915	777	428	0.19	39	0.15	40.2	56	40	bdl	44	35	95			
	02/11/2016	18.7	7.1	84	1088	1030	647	0.15	54	0.21	6.6	48	47	0.3	63	52	113			
W11	23/03/2016	15.9	7	35	1948	1830	837	0.08	233	0.12	80.7	145	141	1.33	178	89	125			−19.2
	16/05/2016	17.6	7.2	29	1948	1978	930	0.97	203	0.21	85.2	171	146	0.82	197	83	160			
	29/06/2016	17.4	7.1	95	2130	1739	780	0.07	188	0.04	69.3	169	138	bdl	194	75	126			
	02/09/2016	21	6.9	27	2110	1898	992	1.63	171	0.2	25.9	151	129	1.01	180	85	162			
	02/11/2016	18.8	6.9	67	2020	1833	952	0.14	154	0.19	6.1	153	130	0.67	193	86	158			
W12	23/03/2016	11.3	7.3	−35	1280	1218	519	0.1	64	0.13	99.1	215	48	0.05	52	37	184			−16.4
	16/05/2016	14.3	7.4	−40	1114	1267	738	0.88	63	0.15	19	113	60	2.7	55	37	176			
	29/06/2016	16.8	7	94	1354	1213	689	0.09	61	0.08	4.7	125	66	0.07	53	40	175			
	02/09/2016	18.8	7.1	−184	1378	1288	775	0.1	61	0.06	0.1	117	63	1.39	51	41	179			
	02/11/2016	16.3	7	72	1350	1299	778	0.18	62	0.13	2.4	98	67	0.46	54	44	192			
W13	28/06/2017	17	7.1	44	na	1175	700	0.25	68	0.3	23.8	91	76	10.8	3	45	157			
W14	28/06/2017	16	7.6	24	na	960	610	0.4	85	0.28	8.8	17	97	3.5	15	44	79			
W15	21/11/2012	14.5	6.9	−156	980	932	537	0.18	36	0.04	8	74	47	bdl	101	24	105			
W16	29/06/2012	13	7.2	264	2690	2133	586	0.24	215	0.14	65	692	135	bdl	47	128	265			
	02/07/2012	20.7	7.2	100	2710	2300	598	0.25	254	0.15	65	783	134	bdl	43	129	294			
W17	02/07/2012	16.5	7.4	−351	3450	2865	1007	0.27	362	0.28	0.03	599	268	4	258	126	241			
	24/07/2012	16.5	7.5	−378	2990	2961	995	0.31	438	0.26	0.16	643	262	2.6	254	126	240			
W18	29/06/2012	17.2	7.1	271	3160	2533	1062	0.15	435	0.29	1.4	294	298	0.02	128	133	181			
	02/07/2012	16	7.3	181	3820	3080	1209	0.16	385	0.28	3.7	642	282	0.13	174	147	237			

measurement of isotopic composition of noble gases ($^{3}He/^{4}He$, ^{20}Ne, $^{40}Ar/^{36}Ar$, $^{38}Ar/^{36}Ar$) was also collected in a stainless-steel flow-through flask equipped with two Swagelok valves to prevent atmospheric contamination and diffusional loss of helium after sampling. Water temperature, electrical conductivity, pH and Eh were measured in the field. Water samples were collected in 125 mL polyethylene bottles, filtered (0.45 μm) in 50 mL polyethylene bottles containing 0.5 mL of 30% Suprapur HCl, and in glass bottles with the addition of $HgCl_2$ for the determination of major anions concentration, major cations concentration and water (δD and $\delta^{18}O$) and TDIC ($\delta^{13}C$-TDIC), respectively.

3.3. Continuous monitoring techniques

Temporal changes in temperature (T), electrical conductivity (EC) and water level (WL) were monitored in four phreatic wells (W4, W8, W10 and W11) by placing a multi-parameter probe close to the bottom of the water column. Data stored in the data loggers were periodically downloaded. At W4, W8 and W11, all three parameters (T, EC and WL) were monitored by means of a Seba Hydrometrie Dipper PTEC high-performance 32-bit measurement data collector (T, EC, WL sensor accuracy of ±0.1 °C, ± 1 mS/cm and ±0.1%, respectively) while at W10, temperature and water-level were monitored using an integrated pressure sensor OTT Orpheus Mini (accuracy for T and WL measurements were ±0.5 °C and ±0.05%, respectively).

3.4. Chemical and isotopic analysis of waters

The analysis of the main ionic species was performed at the University of Florence on an 861 Advanced Compact IC-Metrohm for cations (Na, NH_4, K, Mg, Ca) and a 761 Compact IC-Metrohm for anions (F, Cl, Br, NO_3, SO_4). The HCO_3 concentrations were determined at the University of Florence by acidimetric titration with 0.01 N HCl using a Basic Titrino 794-Metrohm. The analytical errors for IC and AT were <5%.

The $^{18}O/^{16}O$ and $^{2}H/^{1}H$ isotopic ratios (expressed as ‰ vs V-SMOW) in water samples were determined by using a Finnigan Delta PlusXL mass spectrometer according to standard protocols, using EEZ-3 and EEZ-4 as internal standards that were previously calibrated versus V-SMOW and SLAP reference standards. Oxygen isotopes were analyzed using the CO_2–H_2O equilibration method proposed by Epstein and Mayeda (1953). Hydrogen isotopic ratios were measured on H_2 after the reaction of 10 mL of water with metallic zinc at 500 °C (Coleman et al., 1982). The experimental error was ±0.1‰ and ±1‰ for $\delta^{18}O$ and δD values, respectively. Values of δ ^{13}C-TDIC were analyzed at the INGV of Palermo with a Finningan Delta Plus XL mass spectrometer after the reaction of 3 mL of water with 2 mL of anhydrous phosphoric acid in vacuo (Salata et al., 2000). The recovered CO_2 was analyzed after a two-step extraction and purification procedures of the gas mixtures by using liquid N_2 and a solid-liquid mixture of liquid N_2 and trichloroethylene (Evans et al., 1993; Vaselli et al., 2006). The analytical error for $\delta^{13}C$-TDIC was ±0.05‰.

3.5. Chemical and isotopic analysis of gases

Inorganic gases (CO_2, N_2, O_2, and Ar) stored in the sampling glass flasks were analyzed using a Shimadzu 15A and a Thermo Focus gas chromatographs both equipped with Thermal Conductivity Detectors (TCD). Methane and light alkanes (C_2H_6, C_3H_8. iso-C_4H_{10}, n-C_4H_{10}) were analyzed using a Shimadzu 14A gas chromatograph equipped with a Flame Ionization Detector (FID). The composition of dissolved gas compounds was calculated based on Henry's law constants, regulating the liquid-gas equilibrium for each volatile compound (Vaselli et al., 2006; Tassi et al., 2008). The C_{4+} hydrocarbons were analyzed by GC-MS (Gas Chromatography coupled with Mass Spectrometry) using the Solid Phase Micro-Extraction (SPME) technique (Arthur and Pawliszyn, 1990) to extract volatile organic compounds (VOCs) from the gas mixture and injected in an Ultra-trace GC-MS (Davoli et al., 2003; Mangani et al., 2003; Florez Menendez et al., 2004). Quantitative analyses were performed using an external standard calibration procedure on the basis of calibration curves constructed measuring the instrumental signal of Accustandard® standard mixtures of compounds pertaining to the following functional groups: aliphatic, cyclic and aromatic compounds (Tassi et al., 2011). The values of the Relative Standard

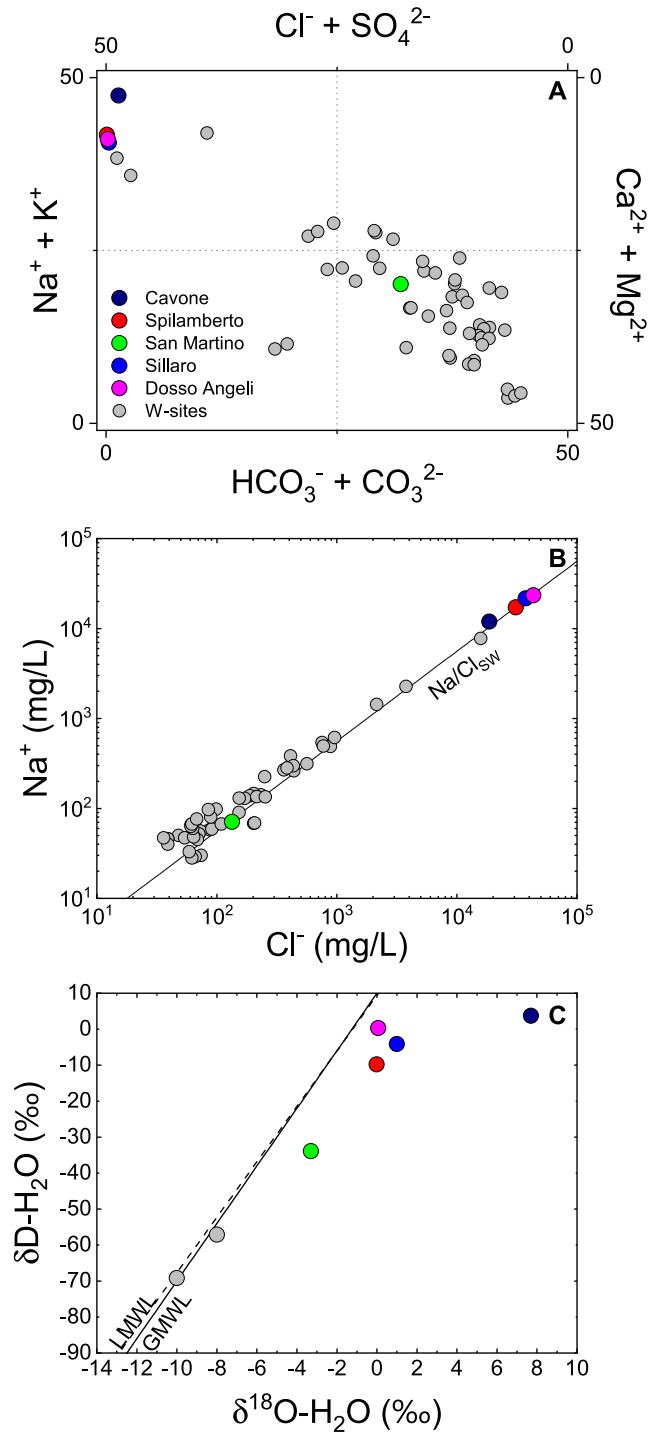

Fig. 4. A) Langelier-Ludwig diagram for the collected waters. **B)** Cl^- vs Na^+ correlation plots for the collected waters. Na/Cl ratio of seawater is shown for comparison. **C)** δD-$\delta^{18}O$ scatter plot for the collected waters. The dotted line delineates the Global Meteoric Water line ($\delta D = 8*\delta^{18}O + 10$; Craig, 1961); the dashed line is the Local Meteoric Water Line for Northern Italy ($\delta D = 7.7094*\delta^{18}O + 9.4034$, Longinelli and Selmo, 2003).

Table 3
Chemical and isotopic composition of dissolved and free gases from W and S sites. Concentration of gas species and total gas pressure are expressed in % vol. and bar, respectively. Isotopic compositions of H and C are reported in delta notation (‰) relative to V-SMOW and V-PDB, respectively. na = not available.

Name/ID	Date	CO_2	N_2	O_2	Ar	CH_4	C_2H_6	C_3H_8	nC_4H_{10}	iC_4H_{10}	Gas tot.	$\delta^{13}C–CO_2$	$\delta^{13}C–CH_4$	$\delta D–CH_4$
	d.m.y.	%	%	%	%	%	%	%	%	%	bar	‰	‰	‰
W1	28/06/2017	2.3	11.5	0.1	0.3	85.8	0.016	0.0025	0.0087	0.0065			−75	
W2	11/07/2014	0.71	3.38	0.01	0.06	95.75	0.03	0.0019	0.00105	0.0013		−15.5	−78	
W3	21/02/2013	na	na	na	na	na	na	na	na	na	na	na	na	na
W4	23/03/2016		85.5	12.4	2.1						0.85			
	16/05/2016		80.3	17.7	2.0						0.85			
	29/06/2016		86.5	11.3	2.2						0.87			
	02/09/2016		92.8	4.9	2.3						0.71			
	02/11/2016		87.6	10.3	2.1						0.72			
W5	16/05/2016	12.4	28.3	0.9	0.7	57.7	0.040	0.007	0.002	0.002	0.88		−65.6	
	29/06/2016	10.1	33.2	1.3	0.8	54.5	0.037	0.006	0.001	0.002	0.84			
	02/09/2016	9.6	25.9	0.7	0.6	63.0	0.038	0.007	0.001	0.002	0.81			
	02/11/2016	11.9	18.7	0.5	0.4	68.4	0.040	0.007	0.003	0.003	0.80			
W6	02/09/2016	1.7	83.5	3.9	2.0	8.8					0.64			
W7	20/09/2016		93.4	4.4	2.2						0.59			
W8	22/10/2015	7.5	76.6	13.9	1.8	0.16					0.96	−23.2	−23.2	−58
	28/10/2015	4.2	78.5	15.1	2.0	0.21					0.91	−23.5	−20.7	
	23/03/2016		65.7	32.8	1.5						0.94			
	16/05/2016		68.6	29.7	1.7						0.83			
	29/06/2016		66.9	31.4	1.7						0.99			
	02/09/2016		60.4	38.0	1.6						1.03			
	02/11/2016		66.8	31.5	1.7						0.76			
W9	28/10/2015	5.0	20.4	0.4	0.5	73.7	0.035	0.004	0.002	0.004	1.36	−32.8	−71.4	−130
	23/03/2016	5.3	28.7	0.5	0.7	65.2	0.041	0.006	0.001	0.002	1.34		−75.3	−177
	16/05/2016	5.8	27.2	0.5	0.6	65.8	0.039	0.006	0.001	0.002	1.14			
	29/06/2016	5.9	27.7	0.9	0.7	64.8	0.038	0.006	0.001	0.002	1.27			
	02/09/2016	1.8	32.5	0.7	0.8	63.5	0.032	0.004	0.001	0.002	1.28			
W10	28/10/2015		68.4	29.8	1.8						0.89			
	23/03/2016		93.9	3.9	2.2	0.03					0.78			
	03/05/2016		91.5	6.4	2.2						0.75			
	11/05/2016		94.2	3.6	2.2	0.05					0.69			
	29/06/2016		96.3	1.3	2.4	0.08					0.63			
	02/11/2016		95.4	2.1	2.4	0.11					0.53			
W11	23/03/2016	51.9	28.8	0.8	0.7	18.5	0.011	0.002	0.001	0.002	1.76		−55.8	−154
	16/05/2016	62.4	10.9	0.4	0.3	26.1	0.011	0.003	0.002	0.002	1.38			
	29/06/2016	60.5	17.1	0.5	0.4	21.5	0.013	0.002	0.001	0.002	1.35			
	02/09/2016	53.5	34.9	1.3	0.9	9.4	0.007	0.002	0.001	0.002	1.17			
	02/11/2016	56.4	18.8	0.5	0.4	23.8	0.020	0.003	0.003	0.003	1.38			
W12	23/03/2016		66.8	31.6	1.6						0.75			
	16/05/2016		66.9	31.6	1.5						0.79			
	29/06/2016		65.5	32.7	1.8						0.73			
	02/09/2016		64.5	33.9	1.6						0.92			
	02/11/2016		65.9	32.4	1.7						0.83			
W13	28/06/2017	1.1	7.4	1.2	0.2	90.1	0.021	0.0036	0.0015	0.0021			−65	
W14	28/06/2017	1.3	8.5	1.0	0.2	89.0	0.021	0.0011						
W15	21/11/2012	7.27	2.86	0.03	0.07	89.82						−20.7	−78.6	−198
W16	29/06/2012	8.2	63.9	1.2	1.5	25.3						−21.3	−50.8	−237
	02/07/2012	47.5	34.0	17.7	0.8	0.014								
W17	02/07/2012	9.13	45.11	1.63	1.09	43.04						−22.9	−51.6	−225
	24/07/2012	81.06	10.16	0.15	0.25	8.58								
W18	29/06/2012	7.48	56.48	1.48	1.37	33.19						−23.1	−56.4	−231
	02/07/2012	86.96	10.59	2.19	0.25	0.01								
S1	08.2015											−72	−68.2	−116
	08.2015											−73.2	−73.2	−156
S2	10.2014	1.99	17.43	4.54	0.40	75.69	0.041	0.0051	0.0021	0.0035		−24.6	−67.5	−188
	11.2015											−35.2	−67.5	−188
S3	08.2014	2.39	24.48	2.82	0.54	69.71	0.051	0.0056	0.0026	0.0041		−16.1	−79	

Deviation (RSD), calculated from five replicate analyses of the gas mixture in which the compounds of interest are present at a concentration of 50 ppbv, were ≤5%. The limit of quantification (LOQ) was determined by linear extrapolation from the lowest standard in the calibration curve using the area of a peak having a signal/noise ratio of 5 (Mangani et al., 2003). The analyses for the determination of concentration of inorganic and organic gases were performed at the University of Florence. The $^{13}C/^{12}C$ ratios of dissolved CO_2 ($\delta^{13}C–CO_{2(aq)}$) were determined on the basis of those measured in the separated gas phase stored in the headspace of the dissolved gas flasks. The $^{13}C/^{12}C$ values (expressed as $\delta^{13}C–CO_2$‰ vs Vienna Peedee Belemnite (VPDB) were analyzed at the INGV of Palermo by mass spectrometry (Finningan Delta Plus, after a two-step extraction and purification procedure of the gas mixtures by using liquid N_2 and a solid-liquid mixture of liquid N_2 and trichloroethylene. Internal (Carrara and San Vincenzo marbles) and international (National Bureau of Standards (NBS) 18 and NBS 19) standards were used to estimate external precision. The analytical uncertainty and the reproducibility were ±0.05‰ and ±0.1‰, respectively. The determination of $\delta^{13}C$ of CH_4, C_2H_6, C_3H_8, n-C_4H_{10} and i-C_4H_{10} and δD of CH_4 were carried out at the Goethe University of Frankfurt using a GC/TC (ThermoFinnigan) connected to a MAT 253 gas source mass spectrometer (ThermoFisher) following the methods outlined by Fiebig et al. (2015). The external analytical precision was ±0.5‰. The reproducibility of hydrogen and carbon stable isotope

Table 4
Chemical (in % vol.) and isotopic composition of gases from oil and gas fields. Isotopic compositions of H and C are reported in delta notation (‰) relative to V-SMOW and V-PDB, respectively. Reference letters (A-G) have been assigned to studied wells in substitution of real well numbers. These letters do not reflect real well names.

Wells	CH_4	C_2H_6	C_3H_8	n-C_4H_{10}	i-C_4H_{10}	$\delta^{13}C$–CH_4	$\delta^{13}C$–C_2H_6	$\delta^{13}C$–C_3H_8	$\delta^{13}C$-nC_4H_{10}	$\delta^{13}C$-iC_4H_{10}	δD-CH_4
	%	%	%	%	%	‰	‰	‰	‰	‰	‰
Cavone											
A	64.50	11.12	15.89	5.561	2.927	−56.2	−35.6	−31.6	−30.1	−30	−210
Spilamberto											
A	97.82	1.37	0.53	0.118	0.171	−56.9	−28.8	−22.2	−18.9	−21.9	−189
B	97.45	1.55	0.64	0.153	0.206	−57	−28.3	−22.3	−19	−21.7	−187
C	97.54	1.52	0.61	0.139	0.191	−57.1	−28.4	−22.3	−18.9	−21.7	−187
D	96.16	2.35	0.98	0.242	0.276	−54.5	−26.7	−22.1	−18.9	−21.6	−184
E	97.65	1.49	0.57	0.122	0.167	−56.4	−28.4	−22.5	−18.8	−22.2	−187
F	96.97	1.85	0.77	0.185	0.225	−56.3	−27.7	−22.4	−18.8	−21.8	−186
G	97.28	1.62	0.70	0.167	0.225	−57.3	−28.2	−22.3	−18.9	−21.7	−187
San Martino											
A	99.81	0.16	0.01	0.005	0.011	−67.1	−37.9	−22.9	−21.3	−22.5	−188
B	99.74	0.18	0.05	0.006	0.020	−66.4	−36.3	−28	−21.5	−23	−190
Sillaro											
A	99.77	0.09	0.10	0.004	0.024	−63.9	−42.8	−34.1	−27.2	−24.3	−196
Dosso Angeli											
A	99.94	0.04	0.01	0.001	0.005	−71.1	−53.9	−34.7	−26	−25	−171
B	99.95	0.04	0.01	0.001	0.002	−71.7	−56.8	−35.7	−26	−24.8	−171
C	99.88	0.07	0.04	0.002	0.012	−69.1	−47	−32.9	−26.1	−25.1	−183

measurements was better than ±6‰ (1σ) and ±0.3‰ (1σ), respectively.

The determination of He, Ne and Ar concentration and isotopic ratios has been performed in the noble gas laboratory of INGV, Sezione di Palermo. The $^3He/^4He$ ratio was measured by admitting helium (separated from neon) into a split-flight-tube mass spectrometer (GVI Helix SFT), while $^4He/^{20}Ne$ ratio was determined into a multicollector mass spectrometer (Thermo-Helix MC plus, dedicated to Ne analysis), after standard purification procedures (e.g., Rizzo et al., 2016, 2019). The values of the $^3He/^4He$ ratio are expressed as R/R_a (where R_a is the $^3He/^4He$ ratio of air, i.e., 1.39×10^{-6}); the analytical error was generally less than 1%. The R/R_a values were corrected for atmospheric contamination based on the $^4He/^{20}Ne$ ratio (R_c/R_a). The Ar-isotope composition was measured in a multi-collector mass spectrometer (GVI MC), for which the analytical uncertainty was generally less than 0.5%. The uncertainty in the determinations of He, Ne, and Ar elemental contents was less than 5%.

4. Results

4.1. Water chemistry

Temperature (in °C), TDS (Total Dissolved Solids in mg/L), pH, Eh (in mV), concentrations of the main solutes (in mg/L) and isotopic composition of water and TDIC are reported in Table 2. Waters from Cavone, Spilamberto, Sillaro, Dosso Angeli gas fields and abandoned gas wells (W1, W2 and W3) have a Na–Cl composition (Fig. 4a), with Na/Cl ratios close to that of seawater (Fig. 4b), high TDS (4.5–71 g/L) and circumneutral pH (from 6.7 to 7.7), while waters from San Martino have a Ca–HCO_3 composition and low TDS (594 mg/L). Waters from shallow phreatic and artesian wells mostly show a Ca–HCO_3 composition (Fig. 4a). Waters from the wells W4–W18 show temperature and TDS ranging from 10.1 °C to 53.6 °C and from 0.7 g/L to 3 g/L, respectively and are neutral to weakly basic (pH = 6.9–8.1). Eh values are highly variable, ranging from −378 mV to +271 mV. The δD and $\delta^{18}O$ values, measured in seven water samples from gas fields and abandoned gas wells (W2 and W3), range from −69.2‰ to +3.7‰ and from −10‰ to +7.7‰ vs. V-SMOW, respectively (Fig. 4c). Carbon isotopic composition of TDIC of the analyzed waters ranges from −26.9‰ to −5‰.

4.2. Gas chemistry

Concentrations of main gas constituents (CO_2, N_2, Ar, O_2, CH_4 and C_2–C_4 alkanes) in shallow aquifers and seeps and in oil and gas wells are shown in Tables 3 and 4, respectively. The chemical gas composition of the W- and S-sites is highly variable. On the basis of CH_4 content, two groups can be distinguished: i) CH_4-rich gases (W1, W2, W5, W9, W13, W14, W15, S2 and S3); and ii) CH_4-poor gases (W4, W6, W7, W8, W10, W11, W12, W16, W17 and W18). Gases of the former group are dominated by CH_4 (>50% vol.) followed by N_2 (up to 32.5% vol.), CO_2 (up to 12.4% vol.), O_2 (not exceeding 4.5% vol.) and Ar (0.06–0.8% vol.). The CH_4-poor gases are instead characterized by relatively low (<50% vol.) or absent contents of CH_4, high concentrations of atmospheric gases and highly variable CO_2 concentrations (from <1.7 to 87% vol.). C_2–C_4 alkanes (ethane, propane, n-butane and iso-butane) were detected in all CH_4-rich gases and in the W11 dissolved gases, with concentration of ΣC_2-C_4 alkanes ranging from 0.012 to 0.063% vol. Gases from oil and gas wells are dominated by CH_4 concentrations ranging from 64.5 to 99.98% vol. At Cavone, propane is the most abundant alkane of the C_2–C_4 fraction, while at other sites ethane is the main component after CH_4. Up to 70 different C_4–C_{10} hydrocarbons, pertaining to the alkane (33 compounds), cyclic (29 compounds), aromatic (6 compounds) and organosulfur (2 compounds) groups were recognized and quantified (Table 5). The C_{4+} hydrocarbons mainly consist of alkanes and cyclics, while relatively high contents of aromatics were only detected at Cavone. Cyclics having C_5, C_6, C_7 and C_8 rings are mostly methylated, although cyclopentane and cyclohexane represent a significant fraction of the total cyclic abundance in some gases (e.g., 12% and 22%, respectively at Cavone). Few cyclics, showing ethyl, propyl branches and polycyclic compounds, occur, though at concentrations lower than those of unbranched and methylated compounds. Benzene and toluene are the most abundant aromatic compounds. Organosulfur group includes dimethyl sulfide and carbon disulfide, both occurring at trace levels in all investigated gases.

4.3. Isotopic composition of CO_2, CH_4, C_2–C_4 alkanes and noble gases

Measured values of $\delta^{13}C$–CO_2, $\delta^{13}C$–CH_4 and δD-CH_4 in the W- and S-gases (Table 3) vary between −73.2 and −15.5‰, −79 and −20.7‰ and −225 and −58‰, respectively. Carbon and hydrogen isotopic composition of CH_4 from oil and gas wells range from −71.7 to −54.5‰ and from −210 to −171‰, respectively (Table 4). At these sites, carbon isotopic composition of ethane, propane, n-butane and iso-butane varies from −56.8 to −26.7‰, −35.7 to −22.1‰, −27.2 to −18.8‰ and −30 to −21.6‰, respectively (Table 4). At oil and gas wells, the isotopic composition of helium, as Rc/Ra ratio, varies within a narrow range, from 0.014 to 0.04, $^{40}Ar/^{36}Ar$ and $^{38}Ar/^{36}Ar$ ratios range from 292.3 to

Table 5
Chemical composition of C_4–C_{10} hydrocarbons of gases from oil and gas fields of the SPRB. Gas concentrations are in μmol/mol. nd = not detected. Reference letters (A-G) have been assigned to studied wells in substitution of real well numbers. These letters do not reflect real well names.

Organic Compounds	Cavone	Spilamberto							San Martino		Sillaro	Dosso Angeli		
	A	*A*	*B*	*C*	*D*	*E*	*F*	*G*	*A*	*B*	*A*	*A*	*B*	*C*
Aliphatic hydrocarbons														
Iso-Butane	29267	1710	2062	1905	2759	1673	2253	2252	112	203	240	46	22	116
Normal-Butane	55606	1179	1531	1385	2417	1220	1847	1671	53	64	42	10	5.5	23
Butane 2-Methyl	55319	4447	4910	4657	6613	4428	6118	5462	468	530	464	114	56	259
Pentane	56905	902	1093	1062	1863	961	1536	1294	62	56	30	8.2	5.2	21
Butane 2,2-Dimethyl	301	544	599	540	908	521	784	641	46	46	11	7.0	3.7	6.9
Butane 2,3-Dimethyl	nd	nd	nd	nd	nd	nd	nd	nd	nd	nd	nd	79	nd	146
Pentane 2-Methyl	32856	2375	2890	2725	4764	3117	4836	3426	427	308	331	nd	68	nd
Pentane 3-Methyl	16022	2249	2569	2519	3212	2632	3399	2620	435	302	84	19	53	32
Normal-Hexane	117706	1004	1500	1594	2471	1592	2753	1612	244	52	52	8.6	13	20
Pentane 2,2-Dimethyl	110	227	238	212	296	248	317	229	42	27	nd	5.3	6.8	6.1
Pentane 2,4-Dimethyl	948	252	294	247	328	352	357	243	81	50	23	17	11	14
Pentane 3,3-Dimethyl	131	199	272	233	320	256	329	232	56	28	nd	3.3	nd	nd
Pentane 2,3-Dimethyl	4021	767	898	945	1085	1179	1343	939	362	159	113	36	14	52
Hexane 3-Methyl	9336	1964	3001	2886	3320	2913	3580	2270	960	399	127	28	nd	57
Normal-Heptane	16817	382	941	865	1199	666	977	529	149	24	90	5.4	nd	28
Hexane 2,2-Dimethyl	75	42	82	58	135	70	63	46	11	5.0	nd	1.0	nd	nd
Hexane 2,5-Dimethyl	366	127	228	165	244	186	222	161	45	16	15	2.9	nd	5.6
Hexane 2,4-Dimethyl	454	105	183	134	225	161	192	122	34	15	19	5.4	nd	11
Hexane 3,3-Dimethyl	nd	5.9	11	6.7	7.5	6.3	8.6	6.1	2.5	1.4	nd	0.6	nd	2.3
Hexane 2,3-Dimethyl	349	75	157	100	150	118	125	72	32	10	nd	3.2	nd	17
Hexane 3,4-Dimethyl	94	19	46	30	38	31	33	21	9.2	2.7	nd	54	nd	108
Heptane 2-Methyl	2457	435	1018	696	1046	653	810	431	200	39	70	2.9	nd	22
Heptane 4-methyl	795	287	635	472	702	510	521	294	139	36	nd	10	3.8	21
Heptane 3-Methyl	1449	491	1115	691	1031	782	887	477	230	52	nd	1.7	nd	5
Normal-Octane	3137	90	354	270	509	227	330	107	75	11	25	1.6	nd	17
Heptane 2,2-Dimethyl	nd	67	123	71	113	82	77	60	37	nd	nd	nd	nd	nd
Heptane 2,4-Dimethyl	nd	53	144	133	270	168	152	106	28	nd	nd	nd	nd	nd
Heptane 3,5-Dimethyl	241	232	604	335	476	386	389	165	140	27	nd	4.6	nd	13
Octane 2-Methyl	537	213	524	295	382	305	333	156	134	29	112	10	nd	34
Octane 3-Methyl	137	107	246	91	80	167	166	61	52	14	nd	8.2	nd	22
Octane 4-Methyl	184	98	232	107	80	168	163	73	5.2	6.4	nd	nd	nd	1.0
Hexane 2,2,4-Trimethyl	232	48	42	132	59	41	nd	89	13	2.5	nd	nd	5.1	nd
Octane 3,6-Dimethyl	nd	nd	27	14	nd	32	25	nd	10	nd	nd	2.2	nd	9.4
Cyclic hydrocarbons														
Cyclopentane	5405	388	441	255	637	542	766	644	80	44	21	nd	nd	nd
Cyclopentane Methyl	13153	1721	2573	2280	3471	2346	3262	1981	558	335	275	24	38	73
Cyclopentane 1,3-Dimethyl cis	2559	517	838	880	960	782	1015	542	273	116	170	38	5.8	71
Cyclopentane 1,3-Dimethyl trans	1239	385	612	579	717	549	736	404	222	106	210	47	8.0	103
Cyclopentane 1,2-Dimethyl cis	2487	808	1254	1193	1278	1226	1577	850	440	200	338	22	3.1	58
Cyclopentane Ethyl	605	91	202	162	203	162	198	98	80	20	22	2	nd	6
Cyclopentane 1,2,4-Trimethyl	300	220	367	290	317	344	363	211	165	53	128	18	2.6	33
Cyclopentane 1,2,3-Trimethyl	323	359	438	438	548	403	574	514	192	44	242	16	1.9	24
Cyclohexane	9857	2260	3742	3424	4384	3113	4714	2698	994	352	66	11	7.8	24
Cyclohexane Methyl	5670	3164	4980	4439	6349	4940	5872	4693	3161	538	177	14	nd	64
Cyclohexane 1,3-Dimethyl cis	1343	1115	1325	1352	1614	1263	1540	1605	357	52	216	44	4.4	75
Cyclohexane 1,1-Dimethyl	nd	265	467	576	751	373	432	384	92	15	nd	nd	nd	nd
Cyclohexane 1,2-Dimethyl	632	421	473	485	548	489	603	570	144	21	125	9.3	nd	22
Cyclohexane 1,4-Dimethyl cis	108	201	251	226	302	226	266	259	68	10	50	5.2	nd	20
Cyclohexane Ethyl	224	199	311	263	318	247	302	226	85	7.3	nd	nd	nd	nd
Cyclohexane 1,1,3-Trimethyl	395	107	120	108	124	116	132	105	78	22	496	142	10.5	212
Cyclohexane 1,2,3-Trimethyl	69	9.4	13	8.9	12	11	12	9.4	8.3	2.1	50	1.7	nd	3.0
Cyclohexane 1,2,4-Trimethyl	148	38	48	38	38	43	54	38	25	3.4	25	2.2	nd	3.9
Cyclohexane 1,3,5-Trimethyl	nd	8.3	9.1	5.7	20	11	12	6.4	5.6	0.7	nd	1.2	nd	2.7
Cyclohexane 1-Ethyl, 3-Methyl	nd	17	30	36	53	22	24	14	11	1.8	nd	0.0	nd	nd
Cyclohexane 1-Ethyl, 4-Methyl	nd	14	15	8.8	4.4	17	19	10	7.7	1.7	nd	1.0	nd	2.5
Cyclohexane Propyl	nd	11	9.2	4.4	2.5	14	12	5.7	5.1	1.1	nd	0.5	nd	1.1
Cyclohexane 1,1,3,5-Tetramethyl	nd	5.4	4.1	4.8	nd	8.5	6.2	5.3	3.6	0.5	nd	1.3	nd	1.5
Cyclohexane 1,1,2,3-Tetramethyl	nd	nd	nd	1.6	nd	2.7	2.8	nd	2.4	0.9	20	1.7	nd	4.1
Cycloheptane Methyl	nd	nd	nd	nd	nd	nd	nd	nd	nd	nd	45	5.3	nd	13
Cyclooctane Methyl	nd	5.9	7.0	2.6	1.5	2.9	4.6	3.9	3.5	1.3	nd	nd	nd	nd
OctaHydro Pentalene	nd	2.2	7.4	6.5	5.1	6.3	8.2	2.7	4.0	nd	nd	nd	nd	nd
1-H Indene Octahydro	nd	8.8	9.3	4.1	nd	12	10	4.5	5.1	1.4	nd	1.2	nd	1.9
3-Carene	nd	nd	nd	4.6	nd	nd	nd	3.4	nd	nd	nd	nd	nd	nd
Aromatic hydrocarbons														
Benzene	18721	nd	83	229	404	95	139	14	nd	nd	17	7.3	nd	86
Toluene	10001	nd	421	381	1362	143	130	23	nd	nd	nd	nd	nd	30
EthylBenzene	302	nd	160	123	266	63	73	6	59	10	nd	nd	nd	26
p-Xylene	282	nd	nd	nd	nd	nd	nd	nd	nd	nd	nd	1.3	nd	23
o-Xylene	nd	0.4	90	48	85	57	37	nd	41	nd	nd	nd	nd	3.9
Styrene	nd	0.7	47	50	403	44	20	nd	23	nd	nd	nd	nd	nd

(*continued on next page*)

Table 5 (*continued*)

Organic Compounds	Cavone	Spilamberto							San Martino		Sillaro	Dosso Angeli		
	A	*A*	*B*	*C*	*D*	*E*	*F*	*G*	*A*	*B*	*A*	*A*	*B*	*C*
Sulfonated compounds														
Dimethyl sulfide	nd	nd	10	9.4	5.4	3.0	17	nd	nd	nd	14	8.4	11	13
Carbon disulfide	nd	0.2	nd	7.2	nd	20	nd	nd	nd	nd	nd	0.5	nd	nd

Table 6
He, Ne and Ar abundances (in ppm) and isotopes of gases from oil and gas fields. $^{40}Ar^*$ abundance and $^{4}He/^{40}Ar^*$ ratio have been computed for Cavone and Spilamberto gases (see Section 5.1.2. for details on calculation and data interpretation). Reference letters (A-G) have been assigned to studied wells in substitution of real well numbers. These letters do not reflect real well names.

Wells	He	Ne	^{40}Ar	^{38}Ar	^{36}Ar	$^{4}He/^{20}Ne$	R/Ra	Rc/Ra	$^{40}Ar/^{36}Ar$	$^{38}Ar/^{36}Ar$	$^{40}Ar^*$	$^{4}He/^{40}Ar^*$
Cavone												
A	15.50	0.18	212.37	0.13	0.66	88.24	0.044	0.040	319.5	0.1897	16.04	0.97
Spilamberto												
A	23.03	0.09	66.45	0.04	0.21	259.72	0.023	0.021	311.0	0.1869	3.42	6.74
D	17.63	0.20	71.09	0.04	0.23	89.51	0.035	0.031	303.8	0.1887	2.08	8.47
G	23.85	0.03	98.85	0.06	0.32	824.09	0.031	0.031	310.3	0.1873	5.35	4.46
San Martino												
B	17.95	0.32	157.10	0.10	0.53	56.86	0.028	0.022	294.3	0.1879		
Sillaro												
A	9.88	1.82	718.26	0.46	2.43	5.42	0.076	0.018	296.9	0.1880		
Dosso Angeli												
A	2.76	0.08	57.06	0.03	0.19	33.67	0.049	0.040	292.3	0.1871		
B	1.97	0.05	53.53	0.03	0.18	37.95	0.040	0.032	294.6	0.1874		
C	2.56	0.08	78.94	0.05	0.27	33.16	0.023	0.014	292.9	0.1897		

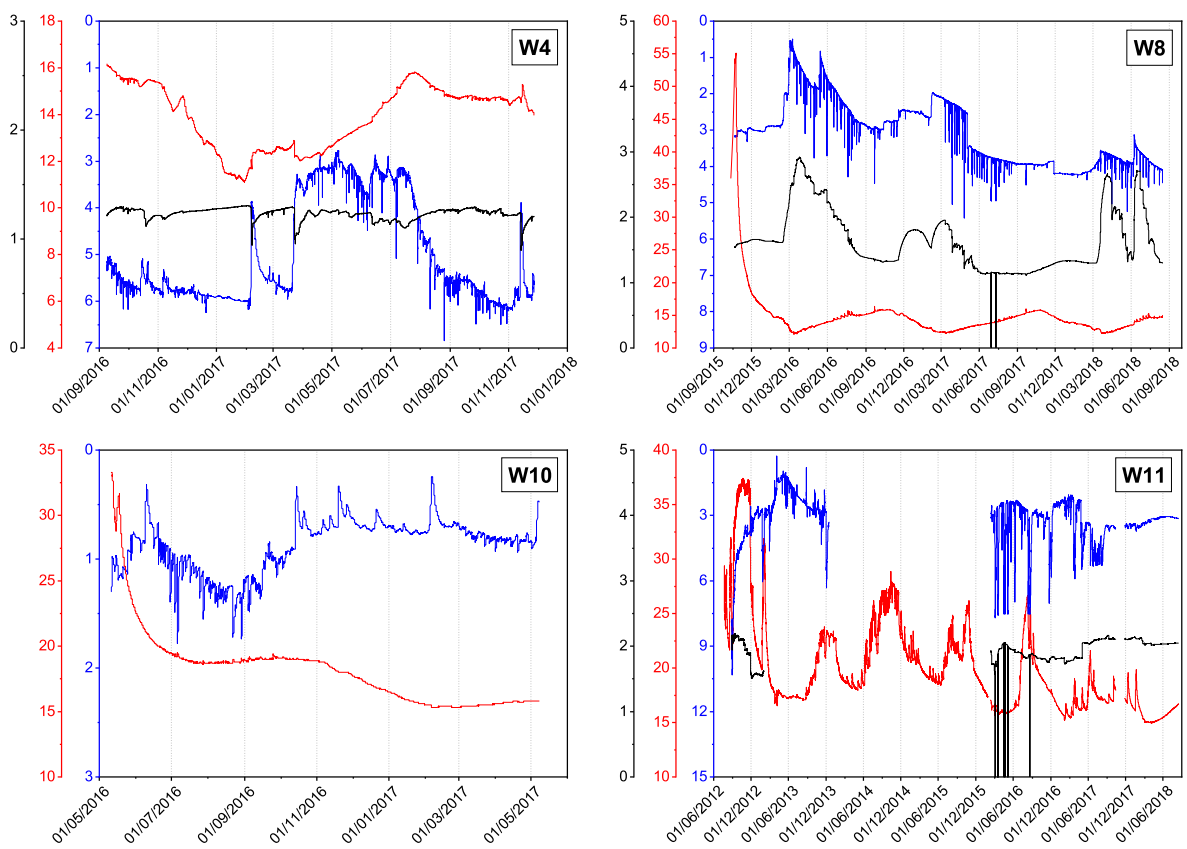

Fig. 5. Temperature (red line and y axis), electrical conductivity (black line and y axis) and water level (blue line and y axis) time series of W4, W8, W10 and W11 wells. The sudden drops in the EC observed in the time series of W8 and W11 are due to the emersion of the probe from the water caused by severe pumping. (For interpretation of the references to colour in this figure legend, the reader is referred to the Web version of this article.)

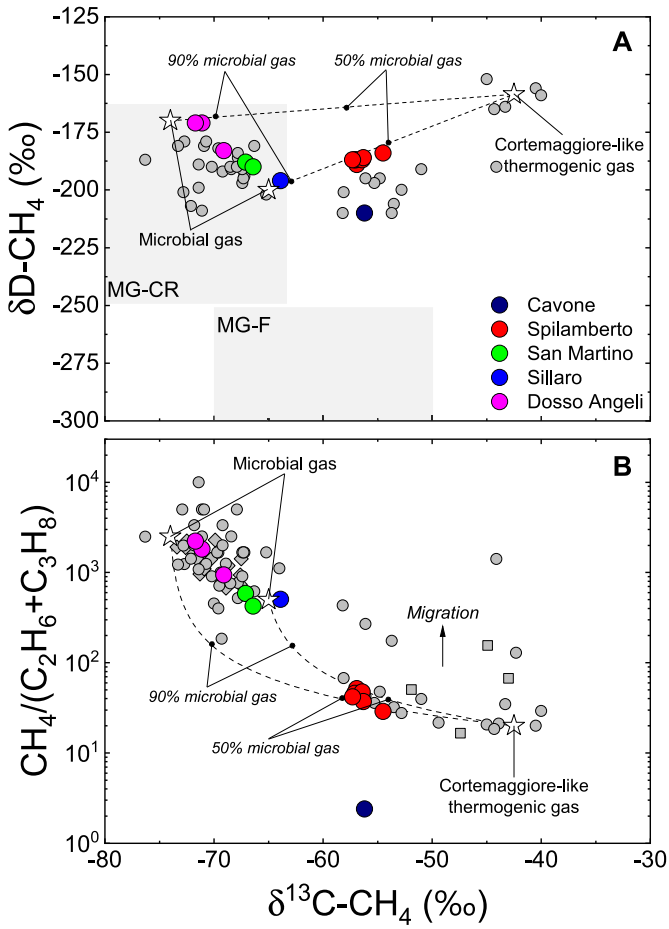

Fig. 6. Chemical and isotopic composition of light hydrocarbons in analyzed gases from oil and gas fields from the SPRB. Data from previous works are also shown as gray symbols (circles, Mattavelli et al., 1983; diamonds, Elliot et al., 1993; squares, Oppo et al., 2013) for cross-comparison. **A)** $\delta^{13}C$–CH_4 vs. δD-CH_4 "Schoell plot" for gas from Emilia-Romagna Region. Compositional fields classically associated to microbial gases are reported (MG-CR: Microbial Gas from Carbonate Reduction; MG-F: Microbial Gas from Fermentation). **B)** Natural gas interpretative diagram combining $CH_4/(C_2H_6 + C_3H_8)$ ratio and stable carbon isotopic composition of CH_4 ($\delta^{13}C$–CH_4). Calculated mixing lines for microbial-thermogenic mixtures are reported. Isotope and molecular composition of Cortemaggiore gas (Mattavelli et al., 1983) has been taken as representative of the thermogenic endmember. Chemical and isotopic composition of microbial gas endmembers are as follows: (1) $CH_4/(C_2H_6 + C_3H_8) = 2500$, $\delta^{13}C$–$CH_4 = -74$‰ and δD-$CH_4 = -170$‰; and (2) $CH_4/(C_2H_6 + C_3H_8) = 500$, $\delta^{13}C$–$CH_4 = -65$‰ and δD-$CH_4 = -200$‰.

319.5 and from 0.1871 to 0.1897, respectively (Table 6). The $^4He/^{20}Ne$ ratio varies from 5.42 to 824.09 (Table 6).

4.4. Temperature, electrical conductivity and water level temporal series

Temperature (in °C), electrical conductivity (EC in mS/cm) and water level (WL as meters below ground level, i.e., mbgl) time series were continuously measured at the four monitored water wells: W4, W8, W10 and W11 and the results are shown in Fig. 5. At well W4, monitored from September 2016 to January 2018, these parameters show no significant changes. The evolution over time of the water temperature shows minimum values in winter and maximum values during summer, thus following a pattern apparently controlled by seasonal cyclicity. Electrical conductivity was mostly constant throughout the monitoring period (≈1.25 mS/cm), while water level changed over time (from 3 to 7 mbgl), with abrupt decreases punctuating the whole period caused by episodes of water pumping for agricultural purposes. At W8 well, where parameters were monitored from October 2015 to August 2018, the water temperature reached 55 °C few days after the installation of the multi-parametric probe and then, exponentially declined to normal values of 14.3 ± 2 °C. The evolution over time of the EC and WL was marked by four episodes of concomitant increase of the two parameters in spring 2016, winter 2017, spring 2018 and summer 2018. As for W4, abrupt decreases of WL marked water pumping episodes for irrigation. At W10 well, monitored from May 2016 to May 2017, water temperature followed the same trend observed for W8, but the maximum recorded value was 33 °C. W11 well has the most peculiar temperature time sequence. In fact, the evolution of the water temperature from September 2012 to August 2018 was punctuated by several heating episodes, with the highest recorded temperature of 36 °C. The minimum water temperature of W11 well for the 2012–2018 period has never dropped below 15 °C, almost 2 °C higher than the average value for a typical phreatic well (Sciarra et al., 2013). Starting from spring 2017, frequency and magnitude of heating episodes at W8 well decreased.

5. Discussion

5.1. Deep hydrocarbon accumulations in the SPRB

5.1.1. Origin and sources of CH_4 and light hydrocarbons

Inspection of the $\delta^{13}C$–CH_4 vs. δD-CH_4 diagram (Schoell, 1980), indicates that CH_4 in San Martino, Sillaro and Dosso Angeli has a predominant (>90%) microbial origin, i.e., deriving from the reduction of CO_2 (Fig. 6a). These data agree with those reported by previous studies (Mattavelli et al., 1983; Elliot et al., 1993) for gases hosted in Pliocene and Pleistocene hydrocarbon reservoirs of the SPRB. Carbon and hydrogen isotopic composition of CH_4 from Spilamberto points to a mixed microbial-thermogenic origin, with a percentage of thermogenic gas of 30–50% (Fig. 6a). This finding is in accordance with results from Mattavelli et al. (1983), who estimated the microbial component to be 30–70%. The thermogenic gas component can be best approximated by gas hosted in the Cortemaggiore reservoir, which shows high content (5–6%) of C_{2+} hydrocarbons and $\delta^{13}C$–CH_4 and δD-CH_4 of around −42.5 ± 2.5‰ V-PDB and −158.5 ± 6.5‰ V-SMOW, respectively (Mattavelli et al., 1983). Carbon and hydrogen isotopic composition of CH_4 from gases of the Cavone reservoir suggests a thermogenic-dominated origin (Fig. 6a). However, as shown in Fig. 6, Spilamberto and Cavone gases are not sourced by the same thermogenic system.

The "Bernard" $\delta^{13}C$–CH_4 vs $CH_4/(C_2H_6 + C_3H_8)$ diagram (Bernard et al., 1977) allows to further distinguish among possible genetic processes, with microbial and early-mature thermogenic gases commonly showing values of $CH_4/(C_2H_6 + C_3H_8)$ ratio >200 and < 100, respectively (Milkov and Etiope, 2018). Gases from oil and gas wells are plotted in Fig. 6b and compared with gases from hydrocarbon reservoirs of the SPRB (Mattavelli et al., 1983; Elliot et al., 1993; Oppo et al., 2013). Gases from Dosso Angeli, San Martino and Sillaro have $CH_4/(C_2H_6 + C_3H_8)$ ratios >400, thus confirming a predominantly microbial origin. However, a minor contribution (<10%) of thermogenic gases at San Martino and Sillaro cannot be ruled out. The content of ethane and propane relative to CH_4 in the Spilamberto gases (Fig. 6b) seems to strengthen the mixing hypothesis between a thermogenic gas, having compositional features similar to gases hosted in the Cortemaggiore reservoir ($\delta^{13}C$–CH_4 and $CH_4/(C_2H_6 + C_3H_8)$ of −42.5‰ and 20, respectively), and a microbial component having $\delta^{13}C$–CH_4 and $CH_4/(C_2H_6 + C_3H_8)$ of around −65‰ and 500, respectively (Mattavelli et al., 1983; Prinzhofer and Pernaton, 1997). As shown in Fig. 6, Cavone gas departs from the thermogenic-microbial mixing trends, owing to higher contents of C_2–C_4 alkanes (32.57%) and consequently lower $CH_4/(C_2H_6 + C_3H_8)$ ratio close to 2.4, thus suggesting that it is genetically different from the Spilamberto gas. As pointed out by Riva et al. (1986), chemical and isotopic features of crude oils hosted in the Cortemaggiore and Cavone reservoirs indicate two different source rocks: Miocene flysch sequence of the Marnoso Arenacea Formation and

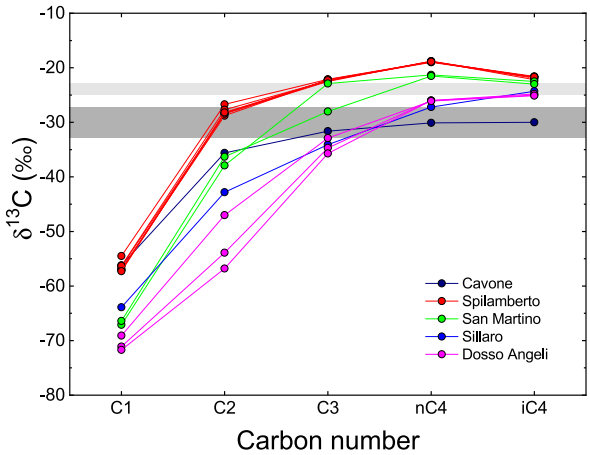

Fig. 7. Carbon isotopic composition of methane and higher chain homologues for the collected gases from oil and gas fields. Stable carbon isotope values of extracts from Triassic (dark gray) and Oligo-Miocene (light gray) source rocks are reported for comparison (Katz et al., 2000).

Triassic carbonates, respectively. Accordingly, the Cavone gas accumulation is likely generated at depth via cracking of organic matter stored in Triassic carbonate rocks (Mattavelli and Novelli, 1990).

Carbon isotopic composition and distribution pattern of light hydrocarbons is a useful indicator of formation mechanism and type and maturity of the source rock (Chung et al., 1988; Clayton, 1991; Rooney et al., 1995; Prinzhofer et al., 2000; Berner and Faber, 1996; Lorant et al., 1998). Gases produced by cracking of organic matter are typically characterized by carbon isotopic distribution coherent with the Rayleigh distillation/fractionation model, where $\delta^{13}C–C_1 < \delta^{13}C–C_2 < \delta^{13}C–C_3 < \delta^{13}C–C_4$ (Dai, 1992; Boreham and Edwards, 2008; Dai et al., 2016). As shown in Fig. 7, all gases show positive carbon isotopic distribution patterns, typical of thermogenic biogenic gases. It is worth noting that microbial gases are almost devoid of C_{2+} hydrocarbons and commonly show values of $\delta^{13}C–C_2H_6$ <-40‰ (Liu et al., 2019). Thus, despite showing a positive carbon isotopic trend, Dosso Angeli and Sillaro gases are of microbial origin. According to Dai et al. (2005), gases with $\delta^{13}C–C_2H_6$ >-27.5‰ and −40‰< $\delta^{13}C–C_2H_6$ <-29‰ were derived from type III (humic) kerogen sources and type I and II (sapropelic) kerogen sources, respectively. Gases with $\delta^{13}C–C_2H_6$ values between −27.5‰ and −29.0‰ are instead of humic-sapropelic mixed thermogenic origin. In this respect, the $\delta^{13}C–C_2H_6$ values of −35.6‰ at Cavone indicates a predominant sapropelic source, as also suggested by the sulfur content and API gravity of crude oil of Cavone, which point to a type II-S kerogen with medium-high sulfur content as the main hydrocarbon source (Riva et al., 1986; Mattavelli and Novelli, 1990; Orr, 2001). The empirical relationships between carbon isotope composition of C_2 and C_3 and maturity (Berner and Faber, 1996), yield vitrinite reflectance (Ro) values of 0.7% for the source rock of Cavone gas. Such value is typical of source rock in the early-stages of oil generation and is in accordance with high wetness ratio (ΣC_2-$C_5/\Sigma C_1$-C_5 = 42) and low C_2/C_3 (0.7), C_2/iC_4 (3.8) and iC_4/nC_4 (0.52) ratios measured at Cavone. At Spilamberto instead, ethane exhibits carbon isotopic compositions ranging from −28.8 to −26.7‰ V-PDB (Table 4), which are ascribable to a sapropelic-humic mixed source rock. This feature could be related to the heterogeneity of the organic matter in the turbiditic clastic rock units forming the inferred source rock of the Marnoso Arenacea Formation (Riva et al., 1986). Accordingly, Oppo et al. (2013) proposed mixing of type-II and –III kerogens as the source of oils and gases hosted in the Salsomaggiore anticline, a hydrocarbon accumulation located 100 km NW of Modena along the Apennine foothills and suggested to have the same source rock as the Cortemaggiore and Spilamberto thermogenic gas.

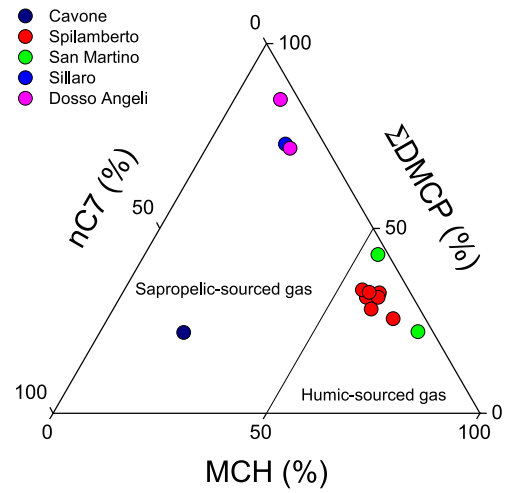

Fig. 8. Ternary plot of C_7 compounds in natural gas from the SPRB. The division of humic- and sapropelic-type gases is after Guoyi et al. (2010). The C_7 compounds refer to heptanes and can be divided into n-heptane (n-C_7), methylcyclohexane (MCH) and dimethylcyclopentane (DMCP). Values of n-C_7 refer to n-C_7/(n-C_7 + MCH + ΣDMCP) ratio. The same applies for fractions of MCH and ΣDMCP.

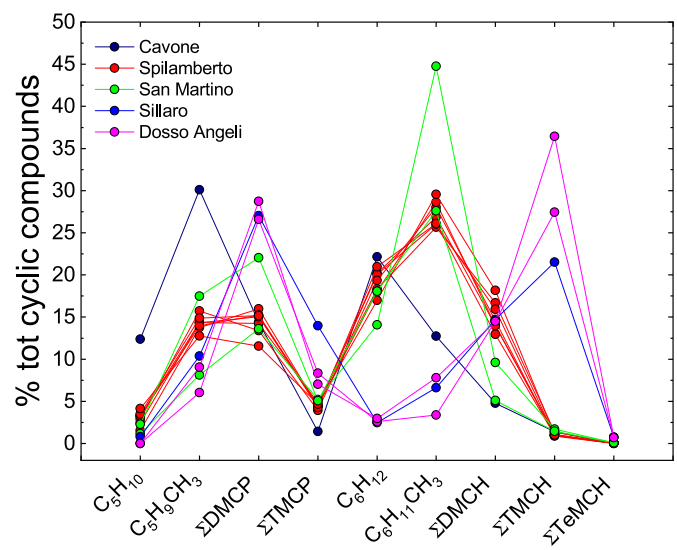

Fig. 9. Concentrations of cyclic compounds with respect to the total cyclic abundance in the investigated gas samples from oil and gas fields of the SPRB.

The relative proportion of the C_7 hydrocarbons, including normal heptane (nC7), dimethylcyclopentane (DMCP) and methylcyclohexane (MCH), is a strong indicator of source rock and maturity (Guoyi et al., 2010). Enrichments in methylcyclohexane are found to occur in oils from terrigenous source material (e.g., lignin, fiber and saccharide of higher plants), whereas high contents of dimethylcyclopentane, mainly deriving from lipids of aquatic organisms, is a typical feature of light hydrocarbons associated with marine-derived oils (Leythaeuser et al., 1979; Dai, 1993; Wang and Zhang, 2008). Normal heptane mainly derives from bacteria and algae, or chain lipoid of higher plants which are the main components of sapropelic organic matter with hydrogen-rich structure (type I and II kerogen). According to these considerations, the relative abundance of C_7 light hydrocarbon compounds can be used to identify the sources of natural gases. In Fig. 8, the Cavone, Sillaro and Dosso Angeli gases show MCH-poor composition, strongly indicating marine/lacustrine organic matter as the main source of light hydrocarbons. Conversely, Spilamberto and San Martino gases are enriched in

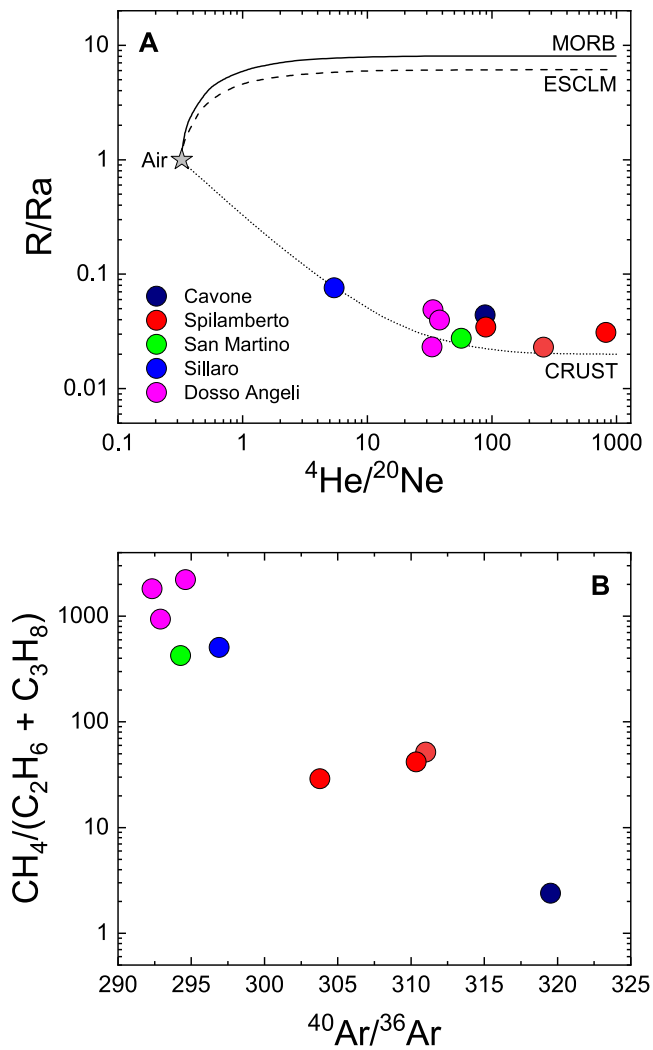

Fig. 10. A) $^{4}He/^{20}Ne$ ratio vs. $^{3}He/^{4}He$ (as R/Ra) diagram. Mixing curves between an air-derived component and a MORB (8 Ra), crustal (0.02 Ra) or European sub-crustal litospheric mantle (ESCLM; 6 Ra) component are reported. **B)** $^{40}Ar/^{36}Ar$ ratio vs. $CH_4/(C_2H_6 + C_3H_8)$ diagram.

methylcyclohexane, as it would be expected for hydrocarbons produced by the thermal decomposition of predominant terrigenous organic matter. Interestingly, Spilamberto and San Martino gases show several geochemical similarities, possibly indicating a common origin of the thermogenic endmember. However, at San Martino reservoir, gases are strongly affected by mixing with microbial gases (mainly CH_4) as well as by biodegradation of C_{2+} alkanes as suggested by high C_2/C_3 and C_2/iC_4 ratios (Prinzhofer and Deville, 2013).

Recent investigations (Tassi et al., 2012; Bonini et al., 2013) found the C_4–C_{10} fraction of thermogenic gases discharged by mud volcanoes and seeps located in the Emilia Apennines enriched in cyclic compounds with respect to alkanes and aromatics. This feature was attributed to the incomplete aromatization of organic matter during thermal maturation at temperatures not exceeding 120–150 °C at >3000 m depth. As observed for the thermogenic gases of the Emilia Apennines, gases hosted in the SPRB reservoirs are markedly enriched in the cyclic fraction. Furthermore, based on the relative concentration of cyclic compounds with respect to the total cyclic abundance (Fig. 9), three main patterns can be distinguished: (i) enrichment in C_6 cyclic compounds (cyclohexane and methycyclopentane) in the Cavone gases; (ii) enrichment in mono- and di-methylated cyclohexane and cyclopentane in the Spilamberto and San Martino gases and (iii) enrichment in dimethylcyclopentane and trimethylcyclohexane in Sillaro and Dosso Angeli gases. The paucity of methylated species and the high contents of aromatic compounds in the Cavone gases may be ascribed to the progressive expulsion of methyl groups from the cyclic rings and the consequent aromatization of the source organic matter as the maturity increases (Tassi et al., 2012).

Cyclic compounds at Spilamberto and San Martino display a pattern approaching those observed for the thermogenic gases discharged from mud volcanoes and seeps at the Emilia Apennines, suggesting a common source rock of a predominant terrigenous origin (likely the Marnoso Arenacea; Lindquist, 1999; Tassi et al., 2012). Degradation of carotenoids during the early stage of organic matter transformation into kerogen could instead be responsible for the high relative concentrations of trimethylcyclohexane in the Sillaro and Dosso Angeli gases. Carotenoids are abundant in marine organic matter and their early diagenetic products mainly consists of tri-methylated cyclohexenyl moieties that may undergo subsequent hydrogenation to form cycloalkanes having three methyl groups attached (Sinninghe Damsté and Koopmans, 1997). The disposition of the methyl groups around the C_6 ring may provide useful insights on the type of the pre-existing carotenoid structure. Sillaro and Dosso Angeli gases are dominated by 1,1,3 trimethylcyclohexane, a common product of degradation of β-carotene (Jiang and Fowler, 1986), a carotenoid typically associated with halotolerant marine algae (e.g., *Dunaliella salina* and *Dunaliella bardawil*) (Soto, 2015). This is consistent with the Na–Cl composition of the saline (TDS >60 g/L) waters at Sillaro and Dosso Angeli and the geological information available on the reservoir rock consisting of sandy sediments deposited in a marine-lagoonal environment during the Pliocene.

Summarizing, three main hydrocarbon reservoirs are present in the deep subsurface of the SPRB (i) microbial gas (e.g., Sillaro and Dosso Angeli): hosted in the Pliocene-Pleistocene marine sediments (ii) Cortemaggiore-like thermogenic dry gas (e.g., Spilamberto); formed within the Marnoso Arenacea Formation at great depth (at least 3 km; Tassi et al., 2012); and (iii) thermogenic gas, cogenetic to early oil, predominantly produced in Triassic carbonate rocks (e.g., Cavone).

5.1.2. Noble gases

Noble gases are useful to further investigate the origin of oil and gas fields (e.g., Ballentine et al., 2002; Barry et al., 2016; Byrne et al., 2018; Liu et al., 2019; Zhang et al., 2019). When looking at the $^{4}He/^{20}Ne$ vs R/Ra ratios (Fig. 10a), it is evident that all gases considered in this study have a $^{3}He/^{4}He$ lower than 0.1 R/Ra, consistent with those of typical crustal fluids (0.01–0.05 Ra (Marty et al., 1993; Ozima and Podosek, 2002). A variable contamination by atmosphere-derived fluids is highlighted by the $^{4}He/^{20}Ne$ values, with the lowest fraction of contamination found in gases from Spilamberto and Cavone. The Rc/Ra values vary in a narrow range (0.014–0.040 Ra, Table 6) typical of crustal fluids, without evident contributions of mantle-derived helium, as recorded in natural gas emissions of the central-northern Apennines (e.g., Sciarra et al., 2019; Smeraglia et al., 2020). The $^{40}Ar/^{36}Ar$ ratio may give further clues on the contribution by atmospheric fluids and radiogenic ^{40}Ar. In our samples, this ratio varies in a narrow range (292–320, Table 6) that is close to the theoretical ratio in atmosphere ($^{40}Ar/^{36}Ar_{atm} = 295.5$; Ozima and Podosek, 2002). Nevertheless, when comparing $^{40}Ar/^{36}Ar$ with $CH_4/(C_2H_6 + C_3H_8)$ a progressive increase of Ar isotopic ratios can be observed at decreasing $CH_4/(C_2H_6 + C_3H_8)$ values (Fig. 10b). At Cavone and Spilamberto, values of $^{40}Ar/^{36}Ar$ ratio higher than 300 indicate a radiogenic, though low, contribution of ^{40}Ar, while the other sites show values of 294.6 ± 2.3, in line with a predominant atmospheric origin of Ar ($^{40}Ar/^{36}Ar_{atm} = 295.5$). Whether the slightly higher $^{40}Ar/^{36}Ar$ values of Spilamberto and Cavone are indicative of degassing of radiogenic Ar over time from the Earth's interior (Renne et al., 2009) or of a decreasing contribution from atmosphere-derived fluids is not easy to assess. In favor of the first hypothesis, we point out that an average age of 3, 20 and 220 Ma for the Pliocene (Dosso

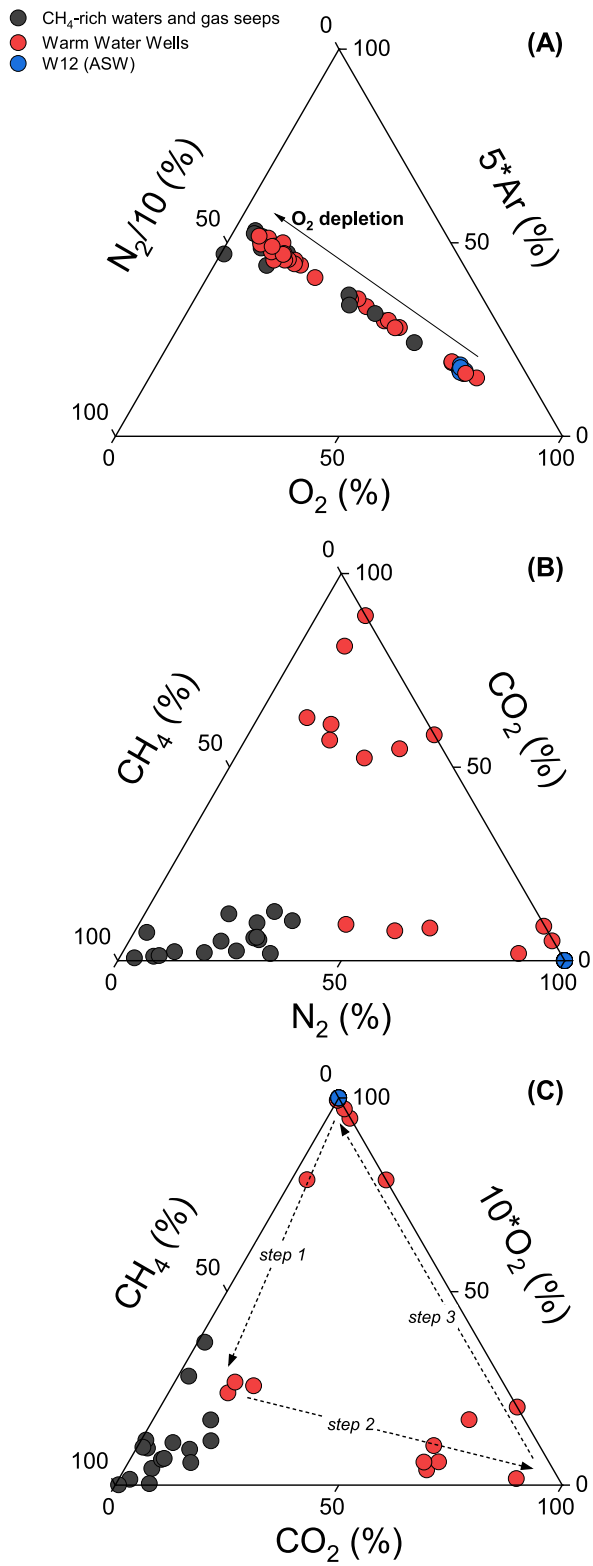

Fig. 11. Ternary plots of chemical composition of gases from water wells (W-sites) and gas seeps (S-sites): **A)** O_2-Ar-N_2 ternary plot **B)** N_2–CO_2–CH_4 ternary plot **C)** CO_2–O_2–CH_4 ternary plot. The three main steps responsible for the water heating episodes are reported and characterized as follows: 1) arrival of external CH_4 into ASW-like waters of shallow aquifers; 2) microbial O_2 and CH_4 consumption followed by CO_2, biomass and heat production; and 3) return to the undisturbed ASW-like conditions.

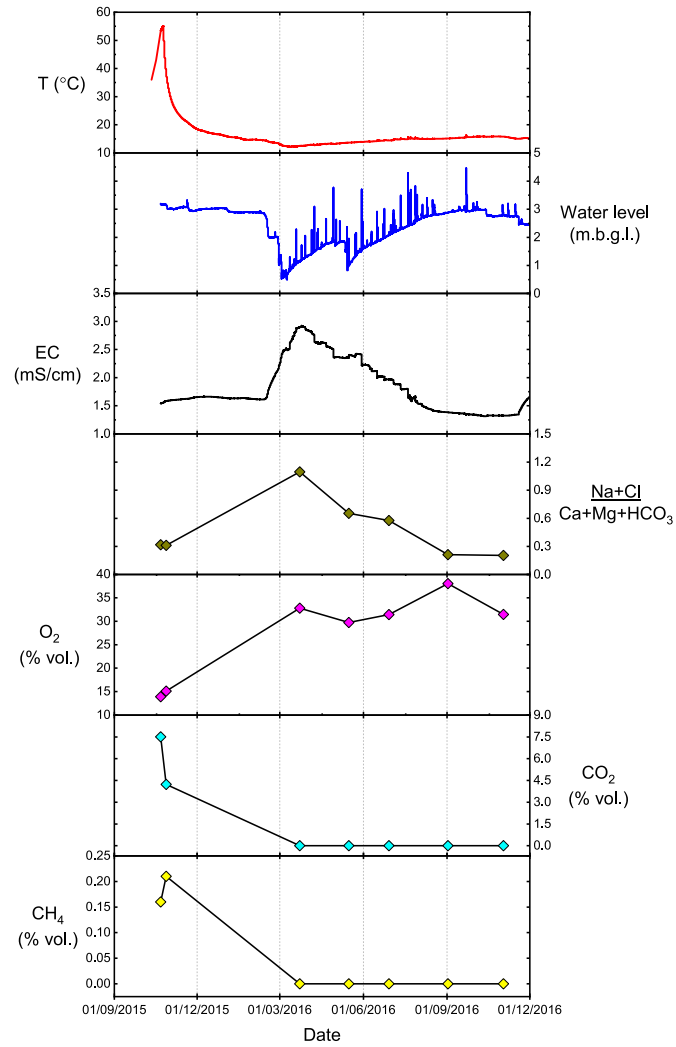

Fig. 12. Multi-panel plot showing time series of some geochemical parameters monitored at water well W8 from September 2015 and December 2016. From top to bottom: water temperature, water level, electrical conductivity, Na + Cl/Ca + Mg + HCO_3 ratio and concentrations of dissolved oxygen (O_2), carbon dioxide (CO_2) and methane (CH_4). Inspection of time series highlights that an increase of dissolved CO_2 and CH_4 concentrations and a co-occurring decrease of O_2 concentration are reported in correspondence of the heating episode of October 2015. On the contrary, the other parameters do not show noticeable changes during the same period.

Angeli and Sillaro), Miocene (Spilamberto and San Martino) and Triassic (Cavone) source fluids has been previously reported (Lindquist, 1999). Nevertheless, an increasing radiogenic production should also favor a progressive increase of $^4He/^{40}Ar^*$ due to the preferential accumulation of radiogenic ^4He with respect to ^{40}Ar (Ballentine et al., 1994; Kim et al., 2008). However, if we compute the $^{40}Ar^*$, which is the amount of ^{40}Ar corrected for the atmospheric contributions ($^{40}Ar^* = {}^{40}Ar_{meas.} - {}^{40}Ar/^{36}Ar_{atm} \times {}^{36}Ar_{meas.}$), only considering $^{40}Ar/^{36}Ar$ values higher than 300, the highest $^4He/^{40}Ar^*$ values are observed in gases from Spilamberto ($^4He/^{40}Ar^* = 4.5$–8.5) rather than in those from Cavone ($^4He/^{40}Ar^* = 1$), opposite to what would be expected in case of an age-dependent process. We suggest that such high values of $^4He/^{40}Ar^*$ for Spilamberto gases might result from molecular fractionation during fluid migration from the source rock to the gas reservoirs, with preferential leakage of ^4He over ^{40}Ar. This explanation would be in accordance with the mixed origin of the gas reservoir (see Fig. 6), and the high $^4He/^{20}Ne$ ratios (up to 824) at Spilamberto.

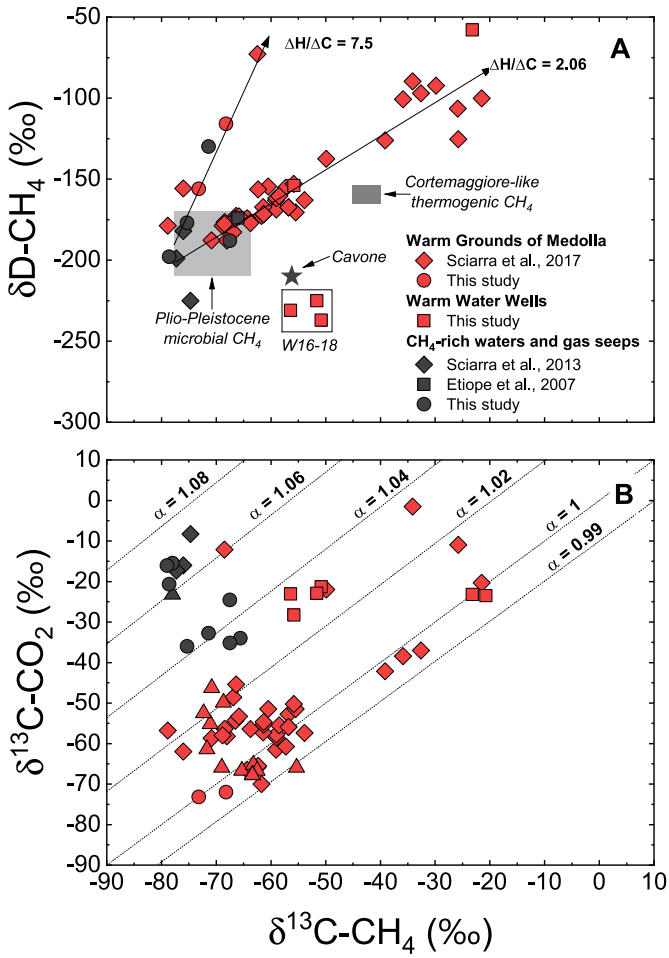

Fig. 13. *Isotopic composition of shallow and surficial gases from the SPRB:* ***A)*** *$\delta^{13}C$–CH_4 vs. δD-CH_4 diagram showing measured values. ^{13}C- D-enrichment trends (black arrow) with angular coefficient, expressed ad ΔH/ΔC (2.06 and 7.5), are also reported. Isotopic composition of Plio-Pleistocene (light gray box), Miocene (dark gray box) and Triassic (Cavone) gases are also shown for comparison (see* Section 5.2.*).* ***B)*** *$\delta^{13}C$–CH_4 vs. $\delta^{13}C$–CO_2 diagram. Multiple lines expressing variable values (0.99–1.08) of CO_2–CH_4 carbon isotope fractionation factor (expressed as α) are also reported.*

5.2. Shallow occurrences of CH_4 in the southern Po river basin

The average value of N_2/Ar ratios (40.9) of the investigated gases does not deviate significantly from that of air saturated water [$(N_2/Ar)_{ASW} = 38$], suggesting both N_2 and Ar have an atmospheric origin (Fig. 11a). On the contrary, oxygen concentration is highly variable. Most of the CH_4-rich gases (dissolved and free) show low oxygen contents with respect to those expected for their N_2 and Ar concentrations, while in dissolved gases from warm water wells (WWW) oxygen concentration ranges from ASW-like values (≈30% vol.) to <0.2% vol. (Fig. 11a). WWW are also characterized by the transient occurrence of CO_2 and CH_4 (Fig. 11b). These evidences seem to suggest the occurrence of an oxygen-consuming process somehow related to the external input of CH_4 and/or CO_2.

The results of our geochemical survey highlighted that in correspondence of water heating episodes, significant concentrations of dissolved CH_4 and CO_2 were detected, along with an abrupt decrease in O_2 concentration, while the water chemistry did not show substantial changes (e.g., W8; Fig. 12). Contribution of warm deep waters from the underlying marine formations as the cause of the temperature increase seems unlikely due to both the low local geothermal gradient (≤20 °C/km) and the absence of any major changes in the water chemistry. During quiescent periods, the chemical composition of the dissolved gas phase in the studied WWW is dominated by atmospheric species (N_2, Ar, and O_2) and resembles that of ASW. This evidences that the sporadic occurrence of CH_4 (and CO_2) in shallow oxic aquifers and the water temperature increase episodes can be ascribed to a common mechanism which might be also responsible for the dissolved oxygen decrease. An identical set of evidences has been previously reported at the Warm Grounds of Medolla (WGM) by Capaccioni et al. (2015). Here, at shallow depth within the soil, metabolic activity of methanotrophic bacteria results in the consumption of free O_2 and diffusively degassing CH_4 and the subsequent production of CO_2, biomass and a relatively large quantity of heat (Capaccioni et al., 2015; Nespoli et al., 2018; Cappelletti et al., 2016). The same microbe-mediated process might be responsible for the observed temperature and dissolved gas chemistry changes at the WWW. The chain of fundamental events possibly occurring at the WWW is depicted in broad terms in Fig. 12c. The three main steps can be described as follows: 1) arrival of external CH_4 into ASW-like waters of shallow aquifers; 2) microbial O_2 and CH_4 consumption followed by CO_2, biomass and heat production; and 3) return to the undisturbed ASW-like conditions (Fig. 12c).

In order to get insights into potential CH_4 sources and sinks, carbon and hydrogen isotopic composition of CH_4 from shallow occurrences and deep reservoirs are compared (Fig. 13a). The $\delta^{13}C$–CH_4 and δD-CH_4 values in CH_4-rich gases (Fig. 13a) range from −79 to −65‰ and from −225 to −130‰, respectively, suggesting a prevailing microbial origin of CH_4. Carbonate reduction and acetate fermentation are the two main metabolic pathways leading to the formation of biogenic CH_4 (Whiticar, 1999). The former process dominates in marine and saline environments, while the latter is typical of freshwater environments where plant root exudates and fresh organic matter provide a ready supply of labile substrate to bacteria (Whiticar, 1999). In freshwater environments, where acetate fermentation dominates over carbonate reduction, carbon isotope ratios of CH_4 and CO_2 are considered to be largely determined by reaction kinetics rather than thermodynamic equilibrium (e.g., Rosenfeld and Silverman, 1959; Nakai, 1960; Claypool and Kaplan, 1974). On the contrary, CO_2–CH_4 carbon isotopic fractionation in gases formed in marine sediments through CO_2-reduction was found to closely approach thermodynamic equilibrium (e.g., Whiticar and Faber, 1986). Moreover, lab-culture experiments reported by Botz et al. (1996) showed that, during the stationary phase, methanogen cultures fractionated carbon isotopes close to the thermodynamic equilibrium between CH_4 and CO_2 in the temperature range of 35–85 °C. As shown in Fig. 13b, most data from CH_4-rich waters show a carbon isotope fractionation factor between CO_2 and CH_4, expressed as $\alpha_{CO2\text{-}CH4}$, ≥1.06. This value is typically associated with CH_4 produced by CO_2-reduction (Whiticar, 1999; Bogard et al., 2014). If we assume isotopic equilibrium between CO_2 and CH_4, such $\alpha_{CO2\text{-}CH4}$ values would yield formation temperatures of around 45 °C, 30–35 °C higher than temperatures directly measured in the CH_4-rich shallow waters (Table 2). Temperatures not significantly exceeding 50 °C were found at depths ranging from 750 to 2000 m in correspondence of the *Dorsale Ferrarese* tectonic fold where the occurrence of gas and salty waters was also reported (Capaccioni et al., 2015). Accordingly, we argue that CH_4 may be produced by microbial carbonate reduction, mostly occurring in sediments associated with seawater or salty waters. Shallow CH_4-rich gas occurrences share many similarities with Plio-Pleistocene biogenic gases. In fact, as shown in Fig. 13a, most of the measured $\delta^{13}C$ and δD values of CH_4, plot close to the compositional field of the Plio-Pleistocene biogenic gases. Furthermore, measured $CH_4/(C_2H_6 + C_3H_8)$ ratios of such gases, ranging from 1015 to 4638, is essentially identical to the values reported for the Plio-Pleistocene biogenic gases. These evidences highly suggest that CH_4 in shallow domains could originate within the Plio-Quaternary marine sediments by CO_2-reduction, then migrates toward the surface and gets stored in shallow anoxic aquifers. Minor and local CH_4 contributions from fermentation of methyl-compounds within near-surface peaty layers cannot totally be excluded, as shown by the

isotopic composition of gases from the W16-18 sites (Fig. 13a).

In Fig. 13a, the distribution of isotopic data from shallow CH_4 occurrences of the SPRB depicts two major trends of ^{13}C-D-enrichment characterized by distinct angular coefficients, expressed as ΔH/ΔC ratio, of 7.5 and 2.06 respectively. Values of ΔH/ΔC ratio ranging from 5.9 to 13 were attributed by several authors (Coleman et al., 1981; Whiticar, 1999; Kinnaman et al., 2007) to microbial oxidation of CH_4, which leaves residual CH_4 enriched in both ^{13}C and D. Few sites, both anoxic aquifers (e.g., W9) and soils from the Warm Grounds of Medolla (WGM), lie on a trend having a ΔH/ΔC of 7.5, consistent with the range suggested for anaerobic oxidation of CH_4 (AOM). This evidence suggests that AOM possibly occurs in O_2-depleted soil horizons and, sporadically, within CH_4-rich aquifers. The other trend has a ΔH/ΔC value of 2.06 and is mostly depicted by data from WGM and WWW. According to Sciarra et al. (2017), the observed distribution of isotopic values is caused by mixing of two sources: (i) a deep (>3000 m depth) Mesozoic thermogenic gas with a^{13}C-enriched CH_4, and (ii) a (200–900 m depth) Plio-Pleistocene shallow microbial gas. However, this hypothesis was formulated without considering carbon and hydrogen isotopic composition of CH_4 from Cavone, which was not available so far. As shown in Fig. 13a, the isotopic composition of CH_4 from known thermogenic reservoirs (Cavone and Cortemaggiore gas accumulations) of the SPRB does not match that of the thermogenic endmember inferred by Sciarra et al. (2017). Thus, we argue that mixing is not a likely explanation, and we propose instead that CH_4 is supplied to WGM and WWW by gases escaping from microbial gas reservoirs hosted in the Plio-Pleistocene sedimentary succession and then is oxidized and isotopically fractionated by the metabolic activity of methanotrophic bacteria at shallow depth and oxic conditions. This implies that Triassic and Miocene gases are not involved in the generation of shallow CH_4 accumulations and gas emissions occurring at the SPRB.

Templeton et al. (2006) suggested that carbon isotope fractionation between CO_2 and CH_4 ($\alpha_{CO2\text{-}CH4}$) caused by aerobic CH_4-oxidizing bacteria strongly correlates to cell density under constant flow conditions. At low cell densities, low concentrations of CH_4 monooxygenase (MMO) limit the amount of CH_4 oxidized, while at higher cell densities, the overall rates of CH_4 oxidation increase. Thus, residual methane is more fractionated at low cell densities than at high cell densities. At WGM, gases with low CH_4 concentrations show a^{13}C- and D-enriched isotopic signature, whereas, at increasing CH_4 concentrations, weak carbon and hydrogen isotope fractionation is observed. Consequently, data previously interpreted as thermogenic could instead be the result of aerobic microbial CH_4 consumption at low cell density. Communities constituted by a small number of individuals could develop during the early stages of growth of bacterial colonies under constant nutrient supply condition, within zones where nutrients are scarce but constantly provided or in environments characterized by cycles of starvation periods and short-lasting pulses of nutrients. We suggest that the second and latter scenarios are more representative of dynamics observed at WGM and during heating episodes of waters at phreatic wells.

Heat release is probably the most peculiar feature of WGM and WWW phenomena. Capaccioni et al. (2015), studying the site of WGM, ascribed temperature anomaly to the metabolic activity of methanotrophic bacteria (Cappelletti et al., 2016). However, high heat production is a feature not commonly associated with methanotrophic activity found in natural environments worldwide. The more Gibbs' free energy is dissipated, the less will be available for biomass or product yield. Under nutrient-limited conditions bacteria can consume higher amounts of energy without concomitant biomass production. In this growth-independent reaction, energy sources were converted to heat (Russell, 1986), i.e., as Westerhoff et al. (1983) theorized: *"thermodynamic efficiency may be sacrificed to make the process run faster"*. Therefore, heat release would be expected to happen in response of a pulse of nutrients after a starvation period. Another explanation can be that wasting of energy source as heat is used for denying substrate to competing organisms or to make environmental temperature unfavorable for the growth of other species (Russell, 1986). The former hypothesis seems to be more consistent with the general view of the nutrients supplying systems at WGM and especially at WWW, but evolutionary reasons cannot be ruled out. However, it is beyond the scope of this study to investigate the environmental microbiology of these sites.

Summarizing, Warm Grounds of Medolla (WGM) can be regarded as biogeochemical system in steady state where microbes are almost constantly fed by biogenic CH_4. On the contrary, heating episodes in water wells record the arrival of discrete amounts of CH_4 into oxic shallow aquifers. In this respect, W11 warm well stands alone among the WWW since CH_4 and CO_2 are always present as dissolved gases, indicating that CH_4 consumption is constantly counterbalanced by a CH_4 input. Finally, where the gas flux is high enough to escape the methanotrophic biofilter, mild to vigorous CH_4 bubbling can occur, as for example at W13-15 water wells.

5.3. *Physical pathways of CH_4-rich fluids in the sedimentary prism of the Southern Po River Basin*

According to the geological setting characteristics of the SPRB, gas sources can be deep marine turbiditic environment, pro-deltaic and lagoonal materials as well as alluvial basin sediments with or without peaty layers. The main gas-hosting sediments are the sandy terms of the Bouma turbiditic sequences and the riverbed and crevasse channel networks in marine and continental environments, respectively. For these reasons, referring in particular to the foreland basin of the Emilia Plain (Fig. 1), the structural traps collected gases in a suite of superimposed reservoirs hosted in the Pliocene marine suite (e.g., Dosso Angeli Field) whose huge total volume available for feeding the reservoirs largely exceeds that of the overlying Pleistocene continental suite nourishing the buried network of paleo-riverbeds.

If the up-dip secondary migration of natural gas in buried syncline contexts (Oppo et al., 2015) is continuous through time also around the crestal area of the eroded, buried thrusts' folds this advection must be assumed as an effective mechanism of gas seep from the structural high top. This could have been the origin the carbonatic cemented horizons often recorded at the base of the sediments directly overlying the eroded tops (e.g., Capaccioni et al., 2017), thus possibly being Methane-Derived Authigenic Carbonates (MDAC; Capozzi et al., 2012; Oppo et al., 2015). Furthermore, upon these eroded structural highs top the existence of brackish groundwaters is recorded resulting from the mixing of Na–Cl connate water and surrounding Ca/Na–HCO_3 groundwaters (Fig. 2). In the Pleistocene and Holocene buried riverbeds net gas collects by means of a prominent sub-horizontal migration along sand body axis and finally can vertically seep at every place where the effectiveness of the stratigraphic seals is lacking due to stratigraphic pinch-outs or secondary discontinuities (Capaccioni et al., 2015, 2017; Cahill et al., 2017). The complex interconnection net of the permeable sedimentary bodies scattered in uppermost part of the local syntheme (Amorosi et al., 2017) is due to the channel size greater than present and to the character of monocursal or anabranching riverbed of paleo-Po during the glacial periods as well as its freely wandering behaviour. In this sense, if a direct outcropping of buried fault planes in the plain is excluded, the most recent (Holocene) fluvial network sedimentation is the most important driving factor for establishing the topographic location of surficial gas seep. Nonetheless, secondary permeability in the whole buried sedimentary prism is of primary importance for gas vertical migration, in particular at shallow depth. The fractures are of different origin (tectonic and non-tectonic) and scale: i) tear/wrench faults orthogonally intersecting the first order thrust arc (see Fig. 1; Nardon et al., 1991; ISPRA, 2015); ii) normal faults often located on the thrusts back-side (Bigi et al., 1990) (Fig. 1) and sometimes in the syncline depocentral area (e.g., Castellarin et al., 2006); extradossal faults located on thrusts top above the fold neutral surface (Lisle et al., 2009; Carminati and Valditacca, 2010); iii) faults originating from sediment differential

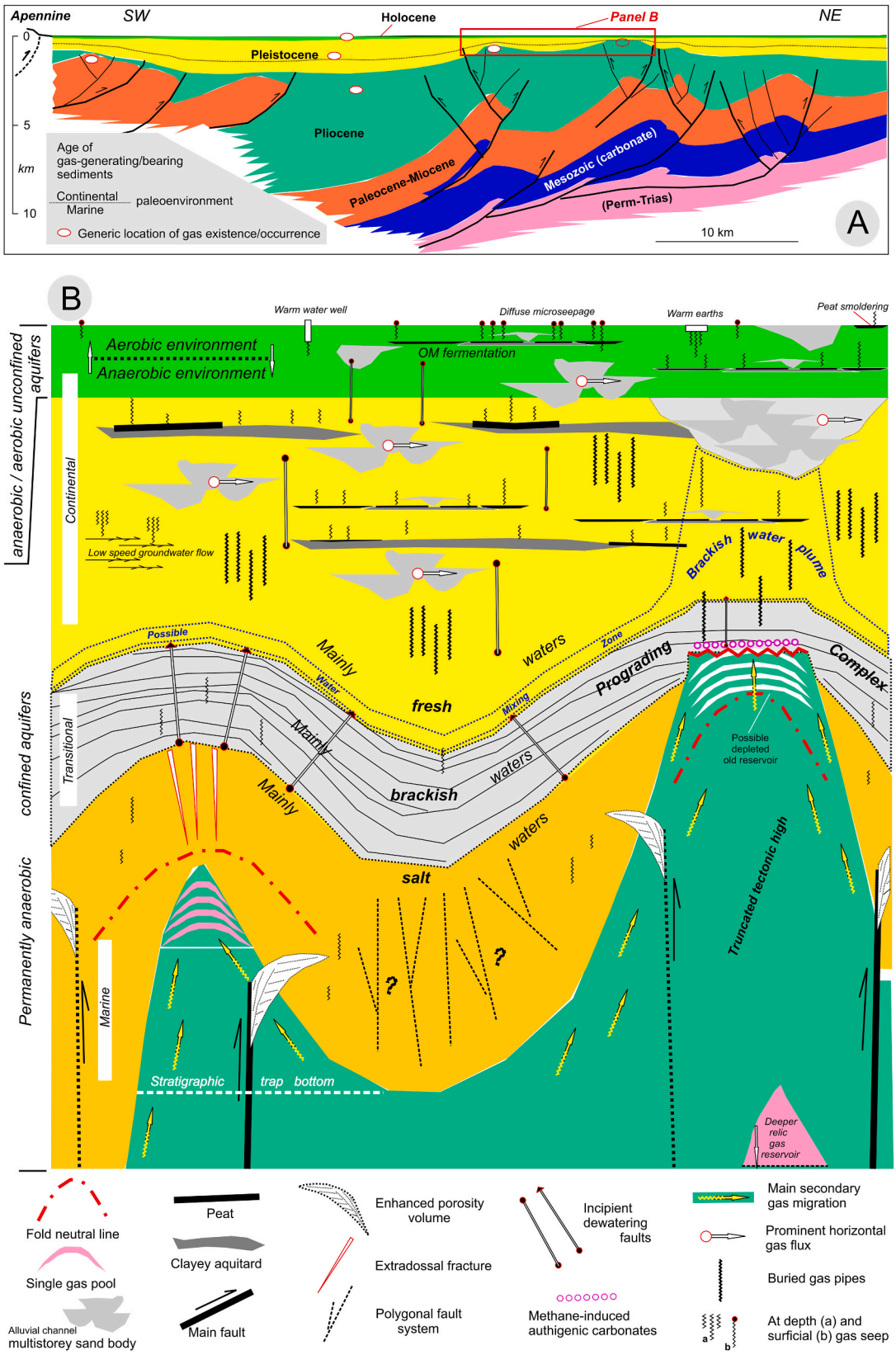

Fig. 14. Conceptual model of the setting of tectonic structures buried beneath the Emilia region alluvial plain. **A)** The age of each single sedimentary body (Paleocene to Holocene) is shown: it also corresponds to the genesis age of related trapped gas. The section results from merging a multiplicity of various subsections (e.g., C–C′ section after Martelli et al., 2017c). **B)** Gather of physical discontinuities kinds possibly existing in the sedimentary prism of Emilia alluvial plain. Furthermore, it is also reported the suggestion that an aliquot of methane can be produced by the bacterial activity in groundwaters slowly circulating through organic matter rich aquifers (Martinelli et al., 2016). Finally, in the same figure surficial peats combustion phenomena linked to methane seep are also indicated according to literature (Cremonini et al., 2008; Martinelli et al., 2012b; Capaccioni et al., 2015).

compaction around the thrusts' top (Carminati and Valditacca, 2010); iv) polygonal faults (Cartwright et al., 2003; Goulty, 2001; Allen et al., 2013; Morgan et al., 2015; Gay, 2017) or incipient sub-surficial dewatering faults (Burst, 1969; Scherer, 1989) and conical faults/fluid pipes (Gay, 2017); v) seismically induced surficial faults (Pratt, 1998; Obermeier et al., 2001). Furthermore, a secondary porosity enhancement can be generated in the sedimentary cover lying above the blind fault tip (Mandl, 1988; Abe et al., 2008). Finally, the aerated surficial zone characterizing today's topographic surface as well as the large number of man-made water wells represents the end-member of an extremely complex network able to deliver gas at seep location. In addition to these disjunction elements other minor structures of seal-breaching (faults, intrusions and pipes) exist allowing vertical migration of fluids (Cartwright et al., 2007). Even if all of them would be lacking a fluid could be carried through an impermeable seal in short (less than a century) events of expulsion when the fluid pressure becomes higher than 85% of the local lithostatic pressure (Roberts and Nunn, 1995).

These features are conceptualized and reported in Fig. 14 to suggest the possible complexity of physical pathways available for gas and groundwater flow in the SPRB as well as in other settings (Wood and Sanei, 2016). Furthermore, these pathways can be responsible also for the mixing of old and young gas as sometimes recognized (Cremonini et al., 2008). Part of these features, such as volumes of enhanced porosity above the fault tip, extradossal fractures as well as polygonal fault systems (PFS), cannot yet be recognizable in the up-to-date available seismic sections (ISPRA, 2015) due to their low-resolution character. Nonetheless, some fractures/faults buried at medium depth (50–300 m or more) that do not appear to be directly linked to local tectonic contexts, were reported (e.g., Castellarin et al., 2006; Cremonini, 2010b; Borgatti et al., 2012), thus possibly suggesting the existence of PFS or incipient dewatering fault systems. Other minor but pervasive features such as pipes or small chimneys were recognized in the uppermost thousands of metres of the Po Plain sedimentary prism (Cremonini, 2010b; Cremonini, 2010a).

6. Conclusions

The chemical and isotopic composition of light hydrocarbons of deep gas wells investigated in the present study evidences three main types of gases in the "deep" subsurface of the SPRB: (i) microbial CH_4-rich gases in marine Pliocene-Pleistocene sediments; (ii) Miocene thermogenic gases formed within the Marnoso Arenacea Formation at great depth (at least 3 km); and (iii) early mature thermogenic gases predominantly produced in Triassic carbonate rocks. These three types are effectively distinguished on the basis of the isotopic composition of CH_4 and C_2–C_4 n-alkanes, $CH_4/(C_2H_6+C_3H_8)$ ratio, relative proportion of the C_7 hydrocarbons and relative concentration of cyclic compounds with respect to the total cyclic abundance. Surficial occurrences of CH_4 are sourced exclusively by the Plio-Pleistocene microbial gas accumulations. At shallow levels, CH_4 is mainly stored in anoxic aquifers. Heating episodes of groundwaters (Warm Water Wells, WWW) and soils (e.g., Warm Grounds of Medolla, WGM) record the arrival of CH_4 into oxic shallow domains. Here, CH_4 readily undergoes exothermic microbial oxidation mediated by methanotrophs under aerobic conditions. Our investigation suggests that microbial consumption might be able to bio-sequester significant amounts of deep Plio-Pleistocene CH_4 in the form of CO_2 and biomass. Where the structural architecture of the sedimentary sequence favors fluid migration, enhancing their flux, the methanotrophic biofilter is bypassed and CH_4 is discharged through soil diffuse degassing or via gas bubbling from phreatic wells where the absence of a top seal prevents the accumulation of CH_4 in the aquifer. These observations suggest that microbial activity in shallow oxic aquifers has the potential to consume significant amounts of deep-sourced CH_4. Such process might be widespread in the SPRB subsurface as well as in many others foreland basins worldwide. Finally, the results of our geochemical characterization of the SPRB deep and shallow natural fluids and the preliminary conceptual model of fluid migration pathways proposed in this study will provide a valuable contribution to the ongoing intergenerational effort of tracing the sources and processes of fluids and understanding their relation with seismicity along and in the vicinity of the Apennines.

Declaration of competing interest

The authors declare that they have no known competing financial interests or personal relationships that could have appeared to influence the work reported in this paper.

Data availability

Data will be made available on request.

Acknowledgments

This paper is dedicated to the memory of Prof. Bruno Capaccioni, brilliant colleague and dear friend, who left us too early. This work was financially supported by the Department of Biological, Geological and Environmental Sciences of University of Bologna, Italy (Bologna), the laboratories of Fluid and Rock Geochemistry and Stable Isotope Geochemistry of the Department of Earth Sciences and CNR-IGG of Florence, and the Noble Gas Laboratory of Istituto Nazionale di Geofisica e Vulcanologia (INGV), Itly, Sezione di Palermo. This study has been developed in the framework of the PhD thesis "*Geochemistry of C-bearing gas compounds in natural fluids under crustal conditions: insights into deep and shallow processes*" (A. Ricci, University of Bologna). We are very grateful to the oil and gas companies (ENI, Gas Plus s. p.a. and Northsun) involved in this project for their essential support and for granting us the access to the exploitation fields. Many thanks are due to the local people for kindly granting us the permission to sample their private wells. We are also grateful to Mariano Tantillo for the technical support in isotopic analysis of noble gases. We thank Liu Quanyou for handling this paper, and two anonymous reviewers for helpful reviews.

References

Abe, S., van Gent, H., Urai, J.L., Holland, M., 2008. Discrete element simulations of the formation of open fractures during normal faulting of cohesive materials. Boll. Geofis. Teor. Appl. 49 (Suppl. 2), 298–309.

Allen, C.C., Oehler, D.Z., Etiope, G., Van Rensbergen, P., Baciu, C., Feyzullayev, A., Martinelli, G., Tanaka, K., Van Rooij, D., 2013. Fluid expulsion in terrestrial sedimentary basins: a process providing potential analogs for giant polygons and mounds in the martian lowlands. Icarus 224 (2), 424–432. https://doi.org/10.1016/j.icarus.2012.09.018.

Amorosi, A., Bruno, L., Cleveland, D.M., Morelli, A., Hong, W., 2017. Paleosols and associated channel-belt sand bodies from a continuously subsiding late Quaternary system (Po Basin, Italy): new insights into continental sequence stratigraphy. GSA Bulletin 129 (3/4), 449–463. https://doi.org/10.1130/B31575.1.

Amorosi, A., Maselli, V., Trincardi, F., 2016. Onshore to offshore anatomy of a late Quaternary source-to-sink system (Po Plain-Adriatic Sea, Italy). Earth Sci. Rev. 153, 212–237. https://doi.org/10.1016/j.earscirev.2015.10.010.

Amorosi, A., Pavesi, M., Ricci Lucchi, M., Sarti, G., Piccin, A., 2008. Climatic signature of cyclic fluvial architecture from the Quaternary of the central Po Plain, Italy. Sediment. Geol. 209, 58–68. https://doi.org/10.1016/j.sedgeo.2008.06.010.

Arthur, C.L., Pawliszyn, J., 1990. Solid phase microextraction with thermal desorption using fused silica optical fibers. Anal. Chem. 62, 2145–2148. https://doi.org/10.1021/ac00218a019.

Baciu, C., Caracausi, A., Etiope, G., Italiano, F., 2007. Mud volcanoes and methane seeps in Romania: main features and gas flux. Ann. Geophys. 50, 501–511. https://doi.org/10.4401/ag-4435.

Ballentine, C.J., Mazurek, M., Gautschi, A., 1994. Thermal constraints on crustal rare gas release and migration: evidence from Alpine fluid inclusions. Geochem. Cosmochim. Acta 58 (20), 4333–4348. https://doi.org/10.1016/0016-7037(94)90337-9.

Ballentine, C.J., Burgess, R., Marty, B., 2002. Tracing fluid origin, transport and interaction in the crust. Rev. Mineral. Geochem. 47 (1), 539–614. https://doi.org/10.2138/rmg.2002.47.13.

Barry, P.H., Lawson, M., Meurer, W.P., Warr, O., Mabry, J.C., Byrne, D.J., Ballentine, C. J., 2016. Noble gases solubility models of hydrocarbon charge mechanism in the Sleipner Vest gas field. Geochem. Cosmochim. Acta 194, 291–309. https://doi.org/10.1016/j.gca.2016.08.021.

Bartolini, C., 2003. When did the Northern Apennine become a mountain chain? Quat. Int. 101–102, 75–80. https://doi.org/10.1016/S1040-6182(02)00090-3.

Bernard, B.B., Brooks, J.M., Sackett, W.M., 1977. A Geochemical Model for Characterization of Hydrocarbon Gas Sources in Marine Sediments. Offshore Technology Conference, Houston, USA, pp. 435–438.

Berner, U., Faber, E., 1996. Empirical carbon isotope/maturity relationships for gases from algal kerogens and terrigenous organic matter, based on dry, open-system pyrolysis. Org. Geochem. 24 (10–11), 947–955. https://doi.org/10.1016/S0146-6380(96)00090-3.

Bigi, G., Cosentino, D., Parotto, M., Sartori, R., Scandone, P., Carrozzo, M.T., Luzio, D., Margiotta, C., Quarta, T., 1990. Structural model of Italy and gravity map (1: 500.000). Prog. Final. Geodinamica (Pubblic. n. 114 (6).

Boccaletti, M., Coli, M., Eva, C., Ferrari, G., Giglia, G., Lazzaretto, A., Merlanti, F., Nicolich, R., Papani, G., Post pischhl, D., 1985. Considerations on the seismotectonics of the northern Apennines. Tectonophysics 117, 7–38. https://doi.org/10.1016/0040-1951(85)90234-3.

Boccaletti, M., Corti, G., Martelli, L., 2011. Recent and active tectonics of the external zone of the Northern Apennines (Italy). Int. J. Earth Sci. 100, 1331–1348. https://doi.org/10.1007/s00531-010-0545-y.

Boccaletti, M., Martelli, L., 2004. Note Illustrative Della Carta Sismotettonica Della Regione Emilia-Romagna, Scala 1:250.000, p. 60. Firenze.

Bogard, M.J., Del Giorgio, P.A., Boutet, L., Chaves, M.C.G., Prairie, Y.T., Merante, A., Derry, A.M., 2014. Oxic water column methanogenesis as a major component of aquatic CH_4 fluxes. Nat. Commun. 5, 5350. https://doi.org/10.1038/ncomms6350.

Bonini, M., 2007. Interrelations of mud volcanism, fluid venting, and thrust-anticline folding: examples from the external northern Apennines (Emilia-Romagna, Italy). J. Geophys. Res. 112, B08413 https://doi.org/10.1029/2006JB004859.

Bonini, M., Tassi, F., Feyzullaev, A.A., Aliyev, C.S., Capecchicci, F., Minissale, A., 2013. Deep gas discharged from mud volcanoes of Azerbaijan: new geochemical evidence. Mar. Petrol. Geol. 43, 450–463. https://doi.org/10.1016/j.marpetgeo.2012.12.003.

Bonzi, L., Ferrari, V., Martinelli, G., Severi, P., 2014. Fenomeni geologici inusuali accaduti in occasione della sequenza sismica dell'Emilia nel 2012. In: Poster 2.2, 33rd Convegno Nazionale Gruppo Nazionale di Geofisica della Terra Solida. Bologna, Italy.

Bonzi, L., Ferrari, V., Martinelli, G., Norelli, E., Severi, P., 2017. Unusual geological phenomena in the Emilia-Romagna plain (Italy): gas emissions from wells and the ground, hot water wells, geomorphological variations. A review and an update of documented reports. Boll. Geofis. Teor. Appl. 58 (2), 87–102. https://doi.org/10.4430/bgta0193.

Boreham, C.J., Edwards, D.S., 2008. Abundance and carbon isotopic composition of neopentane in Australian natural gases. Org. Geochem. 39, 550–566. https://doi.org/10.1016/j.orggeochem.2007.11.004.

Borgatti, L., Bracci, E.A., Cremonini, S., Martinelli, G., 2012. Looking for the effects of the May-June 2012 Emilia seismic sequence (Italy): medium-depth deformation structures at the periphery of the epicentral area. Ann. Geophys. 55, 717–725. https://doi.org/10.4401/ag-6131.

Botz, R., Pokojski, H.D., Schmitt, M., Thomm, M., 1996. Carbon isotope fractionation during bacterial methanogenesis by CO_2 reduction. Org. Geochem. 25 (3–4), 255–262. https://doi.org/10.1016/S0146-6380(96)00129-5.

Burst, J.F., 1969. Diagenesis of Gulf Coast clayey sediments and its possible relation to petroleum migration. AAPG (Am. Assoc. Pet. Geol.) Bull. 53, 73–93.

Buttitta, D., Caracausi, A., Chiaraluce, L., Favara, R., Gasparo Morticelli, M., Sulli, A., 2020. Continental degassing of helium in an active tectonic setting (northern Italy): the role of seismicity. Sci. Rep. 10 (1), 1–13. https://doi.org/10.1038/s41598-019-55678-7.

Byrne, D.J., Barry, P.H., Lawson, M., Ballentine, C.J., 2018. Noble gases in conventional and unconventional petroleum systems. Geol. Soc. Lond. Special Publ. 468 (1), 127–149. https://doi.org/10.1144/SP468.5.

Cabassi, J., Tassi, F., Vaselli, O., Fiebig, J., Nocentini, M., Capecchiacci, F., Rouwet, D., Bicocchi, G., 2013. Biogeochemical processes involving dissolved CO_2 and CH_4 at Albano, Averno, and Monticchio meromictic volcanic lakes (Central-Southern Italy). Bull. Volcanol. 75, 683. https://doi.org/10.1007/s00445-012-0683-0.

Cahill, A.G., Steelman, C.M., Forde, O., Kuloyo, O., Ruff, S.E., Mayer, B., Mayer, K.U., Strous, M., Ryann, M.C., Cherry, J.A., Parker, B.L., 2017. Mobility and persistence of methane in groundwater in a controlled-release field experiment. Nat. Geosci. 10, 289–294. https://doi.org/10.1038/ngeo2919.

Campo, B., Amorosi, A., Vaiani, S.C., 2017. Sequence stratigraphy and late Quaternary paleoenvironmental evolution of the Northern Adriatic coastal plain (Italy). Palaeogeogr. Palaeoclimatol. Palaeoecol. 466, 265–278. https://doi.org/10.1016/j.palaeo.2016.11.016.

Capaccioni, B., Coltorti, M., Todesco, M., Cremonini, S., Di Giuseppe, D., Faccini, B., Tessari, U., 2017. Sand volcano generated by a violent degassing from methane-saturated aquifers: the case study of Medolla (Modena, Italy). Eng. Geol. 221, 91–103. https://doi.org/10.1016/j.enggeo.2017.02.027.

Capaccioni, B., Tassi, F., Cremonini, S., Sciarra, A., Vaselli, O., 2015. Ground heating and methane oxidation processes at shallow depth in Terre Calde di Medolla (Italy): observations and conceptual model. J. Geophys. Res. Solid Earth 120, 3048–3064. https://doi.org/10.1002/2014JB011635.

Capozzi, R., Picotti, V., 2002. Fluid migration and origin of a mud volcano in the Northern Apennines (Italy): the role of deeply rooted normal faults. Terra. Nova 14, 363–370. https://doi.org/10.1046/j.1365-3121.2002.00430.x.

Capozzi, R., Guido, F.L., Oppo, D., Gabbianelli, G., 2012. Methane-Derived Authigenic Carbonates (MDAC) in northern-central Adriatic Sea: relationships between reservoir and methane seepages. Mar. Geol. 332–334, 174–188. https://doi.org/10.1016/j.margeo.2012.06.006.

Cappelletti, M., Ghezzi, D., Zannoni, D., Capaccioni, B., Fedi, S., 2016. Diversity of methane-oxidizing bacteria in soils from "hot lands of Medolla" (Italy) featured by anomalous higgh-temperatures and biogenic CO_2 emission. Microb. Environ. 31 (4), 369–377. https://doi.org/10.1264/jsme2.ME16087.

Carminati, E., Martinelli, G., 2002. Subsidence rates in the Po Plain, northern Italy: the relative impact of natural and anthropogenic causation. Eng. Geol. 66, 241–255. https://doi.org/10.1016/S0013-7952(02)00031-5.

Carminati, E., Scrocca, D., Doglioni, C., 2010. Compaction-induced stress variations with depth in an active anticline: northern Apennines, Italy. J. Geophys. Res. 115, B02401 https://doi.org/10.1029/2009JB006395.

Carminati, E., Valditacca, L., 2010. Two- and three-dimensional numerical simulations of the stress field at the thrust front of the northern Apennines, Italy. J. Geophys. Res. 115, B12.

Cartwright, J., Huuse, M., Aplin, A., 2007. Seal bypass systems. AAPG (Am. Assoc. Pet. Geol.) Bull. 91 (8), 1141–1166.

Cartwright, J., James, D., Bolton, A., 2003. The genesis of polygonal faults: a review. Geol. Soc. Lond. Special Publ. 216, 223–244. https://doi.org/10.1144/GSL.SP.2003.216.01.15.

Casero, P., 2004. Structural setting of petroleum exploration plays in Italy. In: Crescenti, V., Offizi, S.D., Merlino, S., Sacchi, L. (Eds.), Geology of Italy, Special Volume of the Italian Geological Society for the IGC 32 Florence-2004, pp. 189–199.

Castellarin, A., 2001. Alps-apennines and Po plain-frontal Apennines relationships. In: Vai, G.B., Martini, I.P. (Eds.), Anatomy of an Orogen. The Apennines and Adjacent MediterraneanBasins, pp. 177–196. London, Kluver.

Castellarin, A., Cantelli, L., Fesce, A.M., Mercier, J.L., Ricotti, V., Pini, G.A., Prosser, G., Selli, L., 1992. Alpine compressional tectonics in the southern Alps. Relationships with the N-Apennines. Ann. Tect. 6, 62–94.

Castellarin, A., Rabbi, E., Cremonini, S., Martelli, L., Piattoni, F., 2006. New insights into the underground hydrology of the eastern Po Plain (northern Italy). Boll. Geofis. Teor. Appl. 47, 271–298.

Cerrina Ferroni, A., Martelli, L., Martinelli, P., Ottria, G., Catanzariti, R., 2002. Note Illustrative Della Carta Geologico-Strutturale dell'Appennino Emiliano-Romagnolo 1:250.000, vol. 112, p. 1. Firenze.

Cesca, S., Braun, T., Maccaferri, F., Passatelli, L., Rivalta, E., Dahm, T., 2013. Source modelling of the M5-6 emilia-romagna, Italy, earthquakes (2012 may 20-29). Geophys. J. Int. 193, 1658–1672. https://doi.org/10.1093/gji/ggt069.

Chiarabba, C., De Gori, P., Valoroso, L., Petitta, M., Carminati, E., 2022. Large extensional earthquakes push-up terrific amount of fluids. Sci. Rep. 12 (1), 1–10. https://doi.org/10.1038/s41598-022-18688-6.

Chiodini, G., Caliro, S., Cardellini, C., Frondini, F., Inguaggiato, S., Matteucci, F., 2011. Geochemical evidence for and characterization of CO_2 rich gas sources in the epicentral area of the Abruzzo 2009 earthquakes. Earth Planet Sci. Lett. 304 (3–4), 389–398. https://doi.org/10.1016/j.epsl.2011.02.016.

Chiodini, G., Cardellini, C., Di Luccio, F., Selva, J., Frondini, F., Caliro, S., Rosiello, A., Beddini, G., Ventura, G., 2020. Correlation between tectonic CO_2 Earth degassing and seismicity is revealed by a 10-year record in the Apennines, Italy. Sci. Adv. 6 (35), eabc2938 https://doi.org/10.1126/sciadv.abc2938.

Chung, H.M., Gormly, J.R., Squires, R.M., 1988. Origin of gaseous hydrocarbons in subsurface environments: theoretical considerations of carbon isotope distribution. Chem. Geol. 71 (1–3), 97–104. https://doi.org/10.1016/0009-2541(88)90108-8.

Claypool, G.E., Kaplan, I.R., 1974. The origin and distribution of methane in marine sediments. In: Natural Gases in Marine Sediments. Springer, Boston, pp. 99–139.

Clayton, C., 1991. Carbon isotope fractionation during natural gas generation from kerogen. Mar. Petrol. Geol. 8 (2), 232–240. https://doi.org/10.1016/0264-8172(91)90010-X.

Coleman, D.D., Risatti, J.B., Schoell, M., 1981. Fractionation of carbon and hydrogen isotopes by methane-oxidizing bacteria. Geochem. Cosmochim. Acta 45 (7), 1033–1037. https://doi.org/10.1016/0016-7037(81)90129-0.

Coleman, M.L., Sheperd, T.J., Rouse, J.E., Moore, G.R., 1982. Reduction of water with zinc for hydrogen isotope analysis. Anal. Chem. 54, 993–995. https://doi.org/10.1021/ac00243a035.

Craig, H., 1961. Isotopic variations in meteoric waters. Science 133, 1702–1703. https://doi.org/10.1126/science.133.3465.1702.

Cremonini, S., 2010a. Can subaerial pockmarks exist? Atti del 2° Workshop Internazionale sui fenomeni di sinkhole "I sinkholes. In: Gli Sprofondamenti Catastrofici Nell'ambiente Naturale Ed in Quello Antropizzato", Roma, 3-4 Dicembre 2009. ISPRA, Roma, pp. 29–34.

Cremonini, S., 2010b. A preliminary overview of sinkholes in the Emilia-Romagna Region (Italy). Atti del 2° Workshop Internazionale sui fenomeni di sinkhole "I sinkholes. In: Gli Sprofondamenti Catastrofici Nell'ambiente Naturale Ed in Quello Antropizzato", Roma, 3-4 Dicembre 2009. ISPRA, Roma, pp. 257–281, 2010.

Cremonini, S., Etiope, G., Italiano, F., Martinelli, G., 2008. Evidence of possible enhanced peat burning by deep-originated methane in the Po River delta plain. J. Geol. 116, 401–413. https://doi.org/10.1086/588835.

Dai, J.X., 1992. Identification and distinction of various alkane gases. Sci. China (Series B) 35, 185–193.

Dai, J.X., 1993. Identification of coal formed gas and oil type gas by light hydrocarbons. Petrol. Explor. Dev. 20 (5), 26–32.

Dai, J.X., Li, J., Luo, X., Zhang, W.Z., Hu, G.Y., Ma, C.H., Guo, J.M., Ge, S.G., 2005. Stable carbon isotope compositions and source rock geochemistry of the giant gas accumulations in the Ordos Basin, China. Org. Geochem. 36, 1617–1635.

Dai, J.X., Ni, Y.Y., Huang, S.P., Gong, D.Y., Liu, D., Feng, Z.Q., Peng, W.L., Han, W.X., 2016. Secondary origin of negative carbon isotopic series in natural gas. J. Nat. Gas Geosci. 27, 1–7. https://doi.org/10.1016/j.jnggs.2016.02.002.

D'Anastasio, E., De Martini, P.M., Selvaggi, G., Pantosti, D., Marchioni, A., Maseroli, R., 2006. Short-term vertical velocity field in the Apennines (Italy) revealed by geodetic

levelling data. Tectonophysics 418, 219–234. https://doi.org/10.1016/j.tecto.2006.02.008.
Davoli, E., Gangai, M.L., Morselli, L., Tonelli, D., 2003. Characterization of odorants emissions from landfills by SPME and GC/MS. Chemosphere 51, 357–368. https://doi.org/10.1016/S0045-6535(02)00845-7.
Delisle, G., von Rad, U., Andruleit, H., von Daniels, C., Tabrez, A., Inam, A., 2002. Active mud volcanoes on- and offshore eastern Makran, Pakistan. Int. J. Earth Sci. 91, 93–110.
Devoti, R., 2012. Combination of coseismic displacement fields: a geodetic perspective. Ann. Geophys. 55 (4) https://doi.org/10.4401/ag-6119.
Devoti, R., Pietrantonio, G., Pisani, A., Riguzzi, F., Serpelloni, E., 2010. Present day kinematics of Italy. J. Virtual Explor. 36 https://doi.org/10.3809/jvirtex.2009.00237.
Di Bucci, D., Angeloni, P., 2013. Adria seismicity and seismotectonics: review and critical discussion. Mar. Petrol. Geol. 42, 182–190. https://doi.org/10.1016/j.marpetgeo.2012.09.005.
Di Dio, G., 1998. Inquadramento geologico della pianura emiliano-romagnola e del margine appenninico padano. In: Regione Emilia-Romagna & ENI-AGIP, Riserve Idriche Sotterranee Della Regione Emilia-Romagna - Relazione Tecnica, p. 120. Firenze.
Di Luccio, F., Chiodini, G., Caliro, S., Cardellini, C., Convertito, V., Pino, N.A., Tolomei, C., Ventura, G., 2018. Seismic signature of active intrusions in mountain chains. Sci. Adv. 4 (1), e1701825 https://doi.org/10.1126/sciadv.1701825.
Doglioni, C., Harabaglia, P., Merlini, S., Monelli, F., Peccerillo, A., Piromallo, A., 1999. Orogens and slab vs. their direction of subduction. Earth Sci. Rev. 45, 167–208. https://doi.org/10.1016/S0012-8252(98)00045-2.
Elliot, T., Ballantine, C.J., O'Nions, R.K., Ricchiuto, T., 1993. Carbon, helium, neon and argon isotopes in a Po Basin (northern Italy) natural gas field. Chem. Geol. 106, 429–440. https://doi.org/10.1016/0009-2541(93)90042-H.
Energy-pedia, 2010. Italy: Po Valley commences production from the Sillaro gas field. on-line available at: https://www.energy-pedia.com/news/italy/po-valley-commences-production-from-the-sillaro-gas-field.
ENI (Ente Nazionale Idrocarburi), 1972. Acque dolci sotterranee. Inventario dei dati raccolti dall'AGIP durante la ricerca di idrocarburi in Italia, p. 914. Roma.
ENI (Ente Nazionale Idrocarburi), 1994. Acque dolci sotterranee. Inventario dei dati raccolti dall'AGIP durante la ricerca di idrocarburi in Italia dal 1971 al 1990, p. 524. Roma.
Epstein, S., Mayeda, T.K., 1953. Variation of the $^{18}O/^{16}O$ratio in natural waters. Geochem. Cosmochim. Acta 4, 213–224. https://doi.org/10.1016/0016-7037(53)90051-9.
Etiope, G., Klusman, R.W., 2002. Geologic emissions of methane to the atmosphere. Chemosphere 49, 777–789. https://doi.org/10.1016/s0045-6535(02)00380-6.
Etiope, G., Martinelli, G., Caracausi, A., Italiano, F., 2007. Methane seeps and mud volcanoes in Italy: gas origin, fractionation and emission to the atmosphere. Geophys. Res. Lett. 34 (14) https://doi.org/10.1029/2007GL030341.
Etiope, G., 2009. Natural emissions of methane from geological seepage in Europe. Atmos. Environ. 43, 1430–1443. https://doi.org/10.1016/j.atmosenv.2008.03.014.
Evans, W.C., Kling, G.W., Tuttle, M.L., Tanyileke, G., White, L.D., 1993. Gas build-up in Lake Nyos, Cameroon: the recharge process and its consequences. Appl. Geochem. 8, 207–221. https://doi.org/10.1016/0883-2927(93)90036-G.
Fantoni, R., Franciosi, R., 2009. Mesozoic extension and cenozoic compression in Po plain and adriatic foreland. Rendiconti online Società Geologica Italiana 9, 28–31.
Fiebig, J., Hofmann, S., Tassi, F., D'Alessandro, W., Vaselli, O., Woodland, A.B., 2015. Isotopic patterns of hydrothermal hydrocarbons emitted from Mediterranean volcanoes. Chem. Geol. 396, 152–163. https://doi.org/10.1016/j.chemgeo.2014.12.030.
Florez Menendez, J.C., Fernandez Sanchez, M.L., Fernandez Martinez, E., Sanchez Uria, J.E., Sanz-Mendez, A., 2004. Static headspace versus head space solid-phase microextraction (HS-SPME) for the determination of volatile organochlorine compounds in landfill leachates by gas chromatography. Talanta 63, 809–814. https://doi.org/10.1016/j.talanta.2003.12.044.
Galli, P., Castenetto, S., Peronace, E., 2012. May 2012 Emilia earthquakes (MW 6, northern Italy): macroseismic effects distribution and seismotectonic implications. Alpine and Mediterranean Quaternary 25 (2), 105–123.
Gay, A., 2017. Are polygonal faults the keystones for better understanding the timing of fluid migration in sedimentary basins? EPJ Web Conf. 140, 12009 https://doi.org/10.1051/epjconf/201714012009.
Ghielmi, M., Minervini, M., Nini, C., Rogledi, S., Rossi, M., 2013. Late Miocene-Middle Pleistocene sequences in the Po Plain—northern Adriatic Sea (Italy): the stratigraphic record of modification phases affecting a complex foreland basin. Mar. Petrol. Geol. 42, 50–81. https://doi.org/10.1016/j.marpetgeo.2012.11.007.
Ghielmi, M., Minervini, M., Nini, C., Rogledi, S., Rossi, M., Vignolo, A., 2010. Sedimentary and tectonic evolution in the eastern Po-plain and northern adriatic sea area from messinian to middle Pleistocene (Italy), in nature and geodynamics of the northern adriatic lithostere. Rend. Fis. Acc. Lincei 21/1, 131–166.
Goulty, N.R., 2001. Polygonal fault networks in fine grained sediments. First Break 19, 69–73.
Gunderson, K.L., Pazzaglia, F.J., Picotti, V., Anastasio, D.A., Kodama, K.P., Rittenour, T., Frankel, K.F., Ponza, A., Berti, C., Negri, A., Sabbatici, A., 2014. Unravelling tectonic and climatic controls on synorogenic growth strata (Northern Apennines. Italy). GSA Bulletin 124 (3–4), 532–552. https://doi.org/10.1130/B30902.1.
Guoyi, H., Jin, L., Xiuqin, S., Zhongxi, H., 2010. The origin of natural gas and the hydrocarbon charging history of the Yulin gas field in the Ordos Basin, China. Int. J. Coal Geol. 81 (4), 381–391.
IRSA (Istituto Ricerca sulle Acque) and CNR (Consiglio Nazionale delle Ricerche), 1982. Indagine sulle falde acquifere profonde della pianura padana. Quaderni Istituto di Ricerca sulle Acque 5–70, 51 - 3/2.
ISPRA, 2015. Assessing subsurface potentials of the Alpine Foreland Basins for sustainable planning and use of natural resources - area Pilota italiana - modello geologico 3D e geopotenziali della Pianura Padana centrale (Progetto GeoMol). Rapporto ISPRA, 234/2015, 104 pp. with appendix. (on line available at: http://www.isprambiente.gov.it/it/pubblicazioni/statistiche-download.
Jiang, Z.S., Fowler, M.G., 1986. Carotenoid-derived alkanes in oils from northwestern China. Org. Geochem. 10 (4–6), 831–839. https://doi.org/10.1016/S0146-6380(86)80020-1.
Katz, B.J., Dittmar, E.I., Ehret, G.E., 2000. A geochemical review of carbonate source rocks in Italy. J. Petrol. Geol. 23 (4), 399–424. https://doi.org/10.1111/j.1747-5457.2000.tb00494.x.
Kim, K.H., Nagao, K., Sumino, H., Tanaka, T., Hayashi, T., Nakamura, T., Lee, J.I., 2008. He–Ar and Nd–Sr isotopic compositions of late Pleistocene felsic plutonic back arc basin rocks from Ulleungdo volcanic island, South Korea: implications for the genesis of young plutonic rocks in a back arc basin. Chem. Geol. 253 (3–4), 180–195. https://doi.org/10.1016/j.chemgeo.2008.05.009.
Kinnaman, F.S., Valentine, D.L., Tyler, S.C., 2007. Carbon and hydrogen isotope fractionation associated with the aerobic microbial oxidation of methane, ethane, propane and butane. Geochem. Cosmochim. Acta 71 (2), 271–283. https://doi.org/10.1016/j.gca.2006.09.007.
Kopf, A., Deyhle, A., Lavrushin, V.Y., Polyak, B.G., Buachidze, G.I., Eisenhauer, A., 2003. Isotopic evidence for deep gas and fluid migration from mud volcanoes in a zone of incipient continental collision (Caucasus, Russia). Int. J. Earth Sci. 92, 407–426.
Kopf, A., Klaeschen, D., Mascle, J., 2001. Extreme efficiency of mud volcanism in dewatering accretionary prisms. Earth Planet Sci. Lett. 189, 295–313. https://doi.org/10.1016/S0012-821X(01)00278-3.
Leythaeuser, D., Schaefer, R.G., Cornford, C.T., Weiner, B., 1979. Generation and migration of light hydrocarbons (C_2-C_7) in sedimentary basins. Org. Geochem. 1 (4), 191–204.
Lindquist, S.J., 1999. Petroleum systems of the Po Basin province of northern Italy and the northern Adriatic Sea: Porto Garibaldi (biogenic), Meride/Riva di Solto (thermal), and Marnoso Arenacea (thermal). US Department of the Interior, US Geological Survey.
Lisle, R.J., Aller, J., Bastida, F., Bobillo-Ares, N.C., Toimil, N.C., 2009. Volumetric strains in neutral surface folding. Terra. Nova 21, 14–20. https://doi.org/10.1111/j.1365-3121.2008.00846.x.
Liu, Q., Wu, X., Wang, X., Jin, Z., Zhu, D., Meng, Q., Huang, S., Liu, J., Fu, Q., 2019. Carbon and hydrogen isotopes of methane, ethane, and propane: a review of genetic identification of natural gas. Earth Sci. Rev. 190, 247–272. https://doi.org/10.1016/j.earscirev.2018.11.017.
Longinelli, A., Selmo, E., 2003. Isotopic composition of precipitation in Italy: a first overall map. J. Hydrol. 270, 75–88.
Lorant, F., Prinzhofer, A., Behar, F., Huc, A.Y., 1998. Carbon isotopic and molecular constraints on the formation and the expulsion of thermogenic hydrocarbon gases. Chem. Geol. 147 (3–4), 249–264.
Mandl, G., 1988. Mechanics of Tectonic Faulting. Models and basic concepts, Amsterdam, p. 407, 1988.
Mangani, G., Berloni, A., Maione, M., 2003. Cold" solid-phase microextraction method for the determination of volatile halocarbons present in the atmosphere at ultratrace levels. J. Chromatogr. A 988 (2), 167–175. https://doi.org/10.1016/s0021-9673(02)02082-4.
Martelli, L., Santulin, M., Sani, F., Tamaro, A., Bonini, M., Rebez, A., Corti, G., Slejko, D., 2017a. Seismic hazard of the Northern Apennines based on 3D seismic sources. J. Seismol. 21, 1251–1275. https://doi.org/10.1007/s10950-017-9665-1.
Martelli, L., Bonini, M., Calabrese, L., Corti, G., Ercolessi, G., Molinari, F.C., Piccardi, L., Pondrelli, S., Sani, F., Severi, P., 2017b. Explanatory Notes of the Seismotectonic Map of the Emilia-Romagna Region and Surrounding Areas, 93pp. with a map.
Martelli, L., Bonini, M., Calabrese, L., Corti, G., Ercolessi, G., Molinari, F.C., Piccardi, L., Pondrelli, S., Sani, F., Severi, P., 2017c. Note Illustrative Della Carta Sismotettonica Della Regione Emilia Romagna Ed Aree Limitrofe (Explanatory Notes of the Seismotectonic Map of the Emila-Romagna Region and Surrounding Areas), vol. 93, p. 1. Bologna.
Martinelli, G., Cremonini, S., Samonati, E., 2012a. Geological and geochemical setting of natural hydrocarbon emissions in Italy. In: Al-Megren, H. (Ed.), Adv. Nat. Gas Tech., pp. 79–120.
Martinelli, G., Cremonini, S., Samonati, E., 2012b. The Peat fires of Italy. In: Stracher, G. B., Prakash, A., Sokol, E.V. (Eds.), Coal & Peat Fires: a Global Perspective, 2 (Photographs and Multimedia Tours). Elsevier, pp. 205–216 (ISBN: 9780444594129).
Martinelli, G., Dadomo, A., Italiano, F., Petrini, R., Slejko, F.F., 2016. Geochemical monitoring of the 2012 Po Valley seismic sequence: a review and update. Chem. Geol. 469, 147–162.
Martinelli, G., Chahoud, A., Dadomo, A., Fava, A., 2014. Isotopic features of Emilia-Romagna region (North Italy) groundwaters: environmental and climatological implications. J. Hydrol. 519, 1928–1938.
Marty, B., Torgersen, T., Meynier, V., O'nions, R.K., De Marsily, G., 1993. Helium isotope fluxes and groundwater ages in the dogger aquifer, paris basin. Water Resour. Res. 29, 1025–1035. https://doi.org/10.1029/93WR00007.
Mattavelli, L., Ricchiuto, T., Grignani, D., Schoell, M., 1983. Geochemistry and habitat of natural gases in Po Basin, northern Italy. AAPG (Am. Assoc. Pet. Geol.) Bull. 67, 2239–2254.
Mattavelli, L., Novelli, L., 1990. Geochemistry and habitat of the oils in Italy (1). AAPG (Am. Assoc. Pet. Geol.) Bull. 74 (10), 1623–1639.

Milkov, A.V., Etiope, G., 2018. Revised genetic diagrams for natural gases based on a global dataset of >20,000 samples. Org. Geochem. 125, 109–120. https://doi.org/10.1016/j.orggeochem.2018.09.002.

Moggia, M., 2016. Caratteristiche idrochimiche delle acque di Occhiobello (RO). Tesi di laurea triennale. Corso di Laurea in Scienze Geologiche della Scuola di Scienze - Università di Bologna, Anno Accademico 2015-2016. Relatore proff. Capaccioni B. e Cremonini S. (inedita).

Molinari, F.C., Boldrini, G., Severi, P., Duroni, G., Rapti Caputo, D., Martinelli, G., 2007. Risorse idriche sotterranee della Provincia di Ferrara, vol. 80, p. 5. Firenze.

Morgan, D.A., Cartwright, J.A., Imbert, P., 2015. Perturbation of polygonal fault propagation by buried pockmarks and the implications for the development of polygonal fault systems. Mar. Petrol. Geol. 65, 157–171. https://doi.org/10.1016/j.marpetgeo.2015.03.024.

Mucciarelli, M., Donda, F., Valensise, G., 2015. Earthquakes and depleted gas reservoirs: which comes first? Nat. Hazards Earth Syst. Sci. 15 (10), 2201–2208.

Muttoni, G., Carcano, Garzanti E., Ghielmi, M., Piccin, A., Pini, R., Rogledi, S., Sciunnach, D., 2003. Onset of major Pleistocene glaciations in the Alps. Geology 31 (11), 989–992.

Nakai, N., 1960. Carbon isotope fractionation of natural gas in Japan. J. Earth Sci. 8 (2), 174–180. Nagoya University.

Nardon, S., Marzorati, D., Bernasconi, A., Cornini, S., Gonfaloni, M., Mosconi, S., Romano, A., Terdich, P., 1991. Fractured carbonate reservoir characterization and modeling a multidisciplinary case study from the Cavone oil field, Italy. First Break 9, 553–565.

Nespoli, M., Belardinelli, M.E., Gualandi, A., Serpelloni, E., Bonafede, M., 2018. Poroelasticity and fluid flow modeling for the 2012 Emilia-Romagna earthquakes: hints from GPS and InSAR data. Geofluids 15. https://doi.org/10.1155/2018/4160570.

Obermeier, S.F., Pond, E.C., Olson, S.M., 2001. Paleoliquefaction Studies in Continental Settings: Geologic and Geotechnical Factors in Interpretations and Back-Analysis. U. S. Geological Survey open-file Report 01-29-2001.

Oppo, D., Capozzi, R., Picotti, V., 2013. A new model of the petroleum system in the Northern Apennines, Italy. Mar. Petrol. Geol. 48, 57–76.

Oppo, D., Capozzi, R., Picotti, V., Ponza, A., 2015. In: Capozzi, R., Negri, A., Reitner, J., Taviani, M. (Eds.), A Genetic Model of Hydrocarbon-Derived Chimneys in Shelfal Fine-Grained Sediments: the Enza River Field, Northern Apennines (Italy), Carbonate Conduits Linked to Hydrocarbon-Enriched Fluid Escape. Marine Petroleum Geology special issue, pp. 555–556.

Orr, W.L., 2001. Evaluating kerogen sulfur content from crude oil properties. In: Isaacs, C.M., Rullkotter, J. (Eds.), The Monterey Formation from Rocks to Molecules. Columbia University Press, New York, pp. 348–367.

Ozima, M., Podosek, F.A., 2002. Noble Gas Geochemistry. Cambridge University Press, Cambridge.

Pezzo, G., De Gori, P., Lucente, F.P., Chiarabba, C., 2018. Pore pressure pulse drove the 2012 Emilia (Italy) series of earthquakes. Geophys. Res. Lett. 45 (2), 682–690. https://doi.org/10.1002/2017GL076110.

Picotti, V., Pazzaglia, F.J., 2008. A new active tectonic model for the construction of the Northern Apennines mountain front near Bologna (Italy). J. Geophys. Res. 113, BO8412. https://doi.org/10.1029/2007JB005307, 2008.

Pieri, M., Groppi, G., 1981. Subsurface geological structure of the Po plain (Italy). C.N.R.-progetto finalizzato geodinamica. Pubbl. n. 414, 13.

Pratt, B.R., 1998. Syneresis cracks: subaqueous shrinkage in argillaceous sediments caused by earthquake-induced dewatering. Sediment. Geol. 117 (1–2), 1–10.

Prinzhofer, A., Pernaton, E., 1997. Isotopically light methane in natural gas: bacterial imprint or diffusive fractionation? Chem. Geol. 142 (3–4), 193–200.

Prinzhofer, A., Mello, M.R., Takaki, T., 2000. Geochemical characterization of natural gas: a physical multivariable approach and its applications in maturity and migration estimates. AAPG Bull. 84 (8), 1152–1172.

Prinzhofer, A., Deville, E., 2013. Origins of hydrocarbon gas seeping out from offshore mud volcanoes in the Nile delta. Tectonophysics 591, 52–61.

Renne, P.R., Cassata, W.S., Morgan, L.E., 2009. The isotopic composition of atmospheric argon and 40Ar/39Ar geochronology: time for a change? Quat. Geochronol. 4 (4), 288–298. https://doi.org/10.1016/j.quageo.2009.02.015.

RER (Regione Emilia-Romagna), 2003. Carta geologica d'Italia, foglio 223 - Ravenna. ISPRA, Servizio Geologico d'Italia - Regione Emilia-Romagna. System Card, Roma. 2 Sheets.

RER, ENI-AGIP, 1998. Riserve Idriche Sotterranee Della Regione Emilia Romagna, vol. 120, p. 9. Firenze.

Riva, A., Salvatori, T., Cavaliere, R., Ricchiuto, T., Novelli, L., 1986. Origin of oils in Po Basin, northern Italy. Org. Geochem. 10 (1–3), 391–400.

Rizzo, A.L., Caracausi, A., Chavagnac, V., Nomikou, P., Polymenakou, P., Mandalakis, M., Kotoulas, G., Magoulas, A., Castillo, A., Lampridou, D., 2016. Kolumbo submarine volcano (Greece): an active window into the Aegean subduction system. Sci. Rep. 6, 28013 https://doi.org/10.1038/srep28013.

Rizzo, A.L., Caracausi, A., Chavagnac, V., Nomikou, P., Polymenakou, P.N., Mandalakis, M., Kotoulas, G., Magoulas, A., Castillo, A., Lampridou, D., Marusczak, N., Sonke, J.E., 2019. Geochemistry of CO_2-rich gases venting from submarine volcanism: the case of kolumbo (hellenic volcanic arc, Greece). Front. Earth Sci. 7, 60. https://doi.org/10.3389/feart.2019.00060.

Roberts, S.J., Nunn, J.A., 1995. Episodic fluid expulsion from geopressured sediments. Mar. Petrol. Geol. 12, 195–202.

Rooney, M.A., Claypool, G.E., Chung, H.M., 1995. Modeling thermogenic gas generation using carbon isotope ratios of natural gas hydrocarbons. Chem. Geol. 126 (3–4), 219–232.

Rosenfeld, W.D., Silverman, S.R., 1959. Carbon isotope fractionation in bacterial production of methane. Science 130 (3389), 1658–1659.

Russell, J.B., 1986. Heat production by ruminal bacteria in continuous culture and its relationship to maintenance energy. J. Bacteriol. 168 (2), 694–701.

Salata, G.G., Roelke, L.A., Cifuentes, L.A., 2000. A rapid and precise method for measuring stable carbon isotope ratios of dissolved inorganic carbon. Mar. Chem. 69, 153–161. https://doi.org/10.1016/S0304-4203(99)00102-4.

Saunois, M., Stavert, A.R., Poulter, B., Bousquet, P., Canadell, J.G., Jackson, R.B., Raymond, P.A., Dlugokencky, E.J., Houweling, S., Patra, P.K., Ciais, P., Arora, V.K., Bastviken, D., Bergamaschi, P., Blake, D.R., Brailsford, G., Bruhwiler, L., Carlson, K. M., Carrol, M., Castaldi, S., Chandra, N., Crevoisier, C., Crill, P.M., Covey, K., Curry, C.L., Etiope, G., Frankenberg, C., Gedney, N., Hegglin, M.I., Höglund-Isaksson, L., Hugelius, G., Ishizawa, M., Ito, A., Janssens-Maenhout, G., Jensen, K.M., Joos, F., Kleinen, T., Krummel, P.B., Langenfelds, R.L., Laruelle, G.G., Liu, L., Machida, T., Maksyutov, S., McDonald, K.C., McNorton, J., Miller, P.A., Melton, J.R., Morino, I., Müller, J., Murguia-Flores, F., Naik, V., Niwa, Y., Noce, S., O'Doherty, S., Parker, R.J., Peng, C., Peng, S., Peters, G.P., Prigent, C., Prinn, R., Ramonet, M., Regnier, P., Riley, W.J., Rosentreter, J.A., Segers, A., Simpson, I.J., Shi, H., Smith, S. J., Steele, L.P., Thornton, B.F., Tian, H., Tohjima, Y., Tubiello, F.N., Tsuruta, A., Viovy, N., Voulgarakis, A., Weber, T.S., van Weele, M., van der Werf, G.R., Weiss, R. F., Worthy, D., Wunch, D., Yin, Y., Yoshida, Y., Zhang, W., Zhang, Z., Zhao, Y., Zheng, B., Zhu, Q., Zhu, Q., Zhuang, Q., 2020. The global methane budget 2000-2017. Earth Syst. Sci. Data 12, 1561–1623. https://doi.org/10.5194/essd-12-1561-2020.

Scherer, G.W., 1989. Mechanics of syneresis I. Theory. J. Non-Cryst. Solids 108, 18–27.

Schoell, M., 1980. The hydrogen and carbon isotopic composition of methane from natural gases of various origins. Geochem. Cosmochim. Acta 44, 649–661.

Sciarra, A., Cinti, D., Pizzino, L., Procesi, M., Voltattorni, N., Mecozzi, S., Quattrocchi, F., 2013. Geochemistry of shallow aquifers and soil gas surveys in a feasibility study at the Rivara natural gas storage site (Po Plain, Northern Italy). Appl. Geochem. 34, 3–22.

Sciarra, A., Cantucci, B., Coltorti, M., 2017. Learning from soil gas change and isotopic signatures during 2012 Emilia seismic sequence. Sci. Rep. 7, 14187 https://doi.org/10.1038/s41598-017-14500-y.

Sciarra, A., Cantucci, B., Ricci, T., Tomonaga, Y., Mazzini, A., 2019. Geochemical characterization of the Nirano mud volcano, Italy. Appl. Geochem. 102, 77–87.

Scicli, A., 1972. L'attività estrattiva e le risorse minerarie della Regione Emilia-Romagna, Fed. In: delle Casse di Risparmio dell'Emilia-Romagna: Unione Reg. delle Camere di Commercio dell'Emilia-Romagna. Artioli Editore, Modena, p. 728.

Scrocca, D., Carminati, E., Doglioni, C., Marcantoni, D., 2007. Slab retreat and active shortening along the central-northern Apennines. In: Thrust Belts and Foreland Basins. Springer, Berlin, Heidelberg, pp. 471–487.

Simeoni, U., Tessari, U., Corbau, C., Tosatto, O., Polo, P., Teatini, P., 2017. Impact of land subsidence due to residual gas production on surficial infrastructures: the Dosso degli Angeli field study (Ravenna, Northern Italy). Eng. Geol. 229, 1–12. https://doi.org/10.1016/j.enggeo.2017.09.008.

Sinninghe Damsté, J., Koopmans, M.P., 1997. The fate of carotenoids in sediments: an overview. Pure Appl. Chem. 69 (10), 2067–2074.

Smeraglia, L., Aldega, L., Bernasconi, S.M., Billi, A., Boschi, C., Caracausi, A., Carminati, E., Franchini, S., Rizzo, A.L., Rossetti, F., Vignaroli, G., 2020. The role of trapped fluids during the development and deformation of a carbonate/shale intra-wedge tectonic mélange (Mt. Massico, Southern Apennines, Italy). J. Struct. Geol. 138, 104086 https://doi.org/10.1016/j.jsg.2020.104086.

Somoza, L., Diaz-del-Río, V., León, R., Ivanov, M., Fernández-Puga, M.C., Gardner, J.M., Hernández-Molina, F.J., Pinheiro, L.M., Rodero, J., Lobato, A., Maestro, A., Vázquez, J.T., Medialdea, T., Fernández-Salas, L.M., 2003. Seabed morphology and hydrocarbon seepage in the Gulf of Cádiz mud volcano area: acoustic imagery, multibeam and ultra-high resolution seismic data. Mar. Geol. 195, 153–176.

Soto, J.O., 2015. Dunaliella identification using DNA fingerprinting intron-sizing method and species-specific oligonucleotides: new insights on Dunaliella molecular identification. In: Handbook of Marine Microalgae, pp. 559–568.

Tassi, F., Capecchiacci, F., Buccianti, A., Vaselli, O., 2011. Sampling and analytical procedures for the determination of VOCs released into Air from natural and anthropogenic sources: a comparison between SPME (Solid Phase Micro Extraction) and ST (Solid Trap) methods. Appl. Geochem. 27 (1), 115–123. https://doi.org/10.1016/j.apgeochem.2011.09.023.

Tassi, F., Vaselli, O., Luchetti, G., Montegrossi, G., Minissale, A., 2008. Metodo per la determinazione dei gas disciolti in acque naturali, vol. 10450. Int Rep CNR-IGG, Florence, p. 11.

Tassi, F., Vaselli, O., Tedesco, D., Montegrossi, G., Darrah, T., Cuoco, E., Mapendano, M. Y., Poreda, R., Delgado Huertas, A., 2009. Water and gas chemistry at Lake Kivu (DRC): geochemical evidence of vertical and horizontal heterogeneities in a multi-basin structure. G-cubed 10 (2). https://doi.org/10.1029/2008GC002191.

Tassi, F., Bonini, M., Montegrossi, G., Capecchiacci, F., Capaccioni, B., Vaselli, O., 2012. Origin of hydrocarbons in gases from mud volcanoes and CH_4-rich emissions. Chem. Geol. 294 (295), 113–126.

Teatini, P., Ferronato, M., Gambolati, G., Gonella, M., 2006. Groundwater pumping and land subsidence in the Emilia-Romagna coastland, Italy: modeling the past occurrence and the future trend. Water Resour. Res. 42 (1) https://doi.org/10.1029/2005WR004242.

Templeton, A.S., Chu, K.H., Alvarez-Cohen, L., Conrad, M.E., 2006. Variable carbon isotope fractionation expressed by aerobic CH_4-oxidizing bacteria. Geochem. Cosmochim. Acta 70 (7), 1739–1752.

Toth, J., Almasi, I., 2001. Interpretation of observed fluid potential patterns in a deep sedimentary basin under tectonic compression: Hungarian Great Plain, Pannonian Basin. Geofluids 1, 11–36.

Turrini, C., Lacombe, O., Roure, F., 2014. Present -day 3D structural model of the Po Valley basin, Northern Italy. Mar. Petrol. Geol. 56, 266–289.

Vai, G.B., 2001. Structure and stratigraphy: an overview. In: Vai, G.B., Martini, I.P. (Eds.), Anatomy of an Orogen. The Apennines and Adjacent Mediterranean Basins. Kluwer Academic, Dordreccht, pp. 15–31.
Vannoli, P., Burrato, P., Valensise, G., 2014. The seismotectonics of the Po plain (Northern Italy): tectonic diversity in a blind faulting domain. Pure Appl. Geophys. 172, 1105–1142. https://doi.org/10.1007/s00024-014-0873-0.
Vaselli, O., Tassi, F., Montegrossi, G., Capaccioni, B., Giannini, L., 2006. Sampling and analysis of volcanic gases. Acta Vulcanol. 18, 65–76.
Ventura, G., Di Giovambattista, R., 2013. Fluid pressure, stress field and propagation style of coalescing thrusts from the analysis of the 20 May 2012 ML 5.9 Emilia earthquake (Northern Apennines, Italy). Terra. Nova 25, 72–78. https://doi.org/10.1111/ter.12007.
Wang, X., Zhang, M., 2008. Compositional and geochemical characteristics of light hydrocarbons for typical marine oils and typical coal-generated oils in China. Chin. J. Geochem. 27, 407–411.
Westerhoff, H.V., Hellingwerf, K.J., Van Dam, K., 1983. Thermodynamic efficiency of microbial growth is low but optimal for maximal growth rate. Proc. Natl. Acad. Sci. USA 80 (1), 305–309.
Whiticar, M.J., 1999. Carbon and hydrogen isotope systematics of bacterial formation and oxidation of methane. Chem. Geol. 161, 291–314. https://doi.org/10.1016/S0009-2541(99)00092-3.
Whiticar, M.J., Faber, E., 1986. Methane oxidation in sediment and water column environments—isotope evidence. Org. Geochem. 10 (4–6), 759–768.
Wood, J.M., Sanei, H., 2016. Secondary migration and leakage of methane from a major tight-gas system. Nat. Commun. 7, 13614.
Zhang, W., Li, Y., Zhao, F., Han, W., Li, Y., Wang, Y., Holland, G., Zhou, Z., 2019. Using noble gases to trace groundwater evolution and assess helium accumulation in Weihe Basin, central China. Geochem. Cosmochim. Acta 251, 229–246.